Journal of
Manufacturing and Materials Processing

MDPI

Review

A Comprehensive Review of High-Pressure Laser-Induced Materials Processing, Part I: *Laser-Heated Diamond Anvil Cells*

Mohamad E. Alabdulkarim, Wendy D. Maxwell, Vibhor Thapliyal and James L. Maxwell *

Department of Engineering (EεMC^2 Labs), La Trobe University, Bendigo, VIC 3550, Australia
* Correspondence: j.maxwell@latrobe.edu.au

Abstract: *Laser-heated diamond anvil cell (LH-DAC)* experimentation has emerged as a leading technique for materials processing at extreme pressures and temperatures. LH-DAC systems are often employed to better characterise the structure and properties of materials in applications ranging from condensed matter physics to geophysical research to planetary science. This article reviews LH-DAC and related laser-based characterisation, as the *first part* of a series within the broader context of all high-pressure laser-induced material processing. In part I of this review, a synopsis of *laser-heated diamond anvil cell* experimental methods, developmental history, fundamental physicochemical processes, and emerging research trends are provided. Important examples of minerals/materials modified during LH-DAC investigations (since their inception) are also tabulated, including key phase transformations, material syntheses, laser parameters, and process conditions—as a reference for the reader and as a guide for directing future research efforts. Note that laser-dynamic-compression within diamond anvil cells (*LDC-DAC experimentation*) and laser-induced reactive chemical synthesis within diamond anvil cells (*LRS-DAC experimentation*) are treated separately, as Parts II and III of this review.

Keywords: high pressure; high temperature; laser heated diamond anvil cells; phase transformations; materials synthesis

Citation: Alabdulkarim, M.E.; Maxwell, W.D.; Thapliyal, V.; Maxwell, J.L. A Comprehensive Review of High-Pressure Laser-Induced Materials Processing, Part I: *Laser-Heated Diamond Anvil Cells*. *J. Manuf. Mater. Process.* **2022**, *6*, 111. https://doi.org/10.3390/jmmp6050111

Academic Editor: Steven Y. Liang

Received: 23 August 2022
Accepted: 23 September 2022
Published: 29 September 2022

1. Introduction

Over the past century, the development of high-pressure methods for materials modification and synthesis has been the focus of considerable research activity [1]. Diamond anvil cells (DACs), developed by Charlie Weir in the mid-20th century [2,3], are presently the most utilised systems for generating pressures greater than 3 GPa within small volumes [2]. Since the first laser-heating of samples in DACs by Takahashi and Bassett [4], the number of high-pressure materials studies, where materials are processed using UV-IR coherent sources (e.g., lasers or synchrotron radiation) has grown steadily over time—and now totals over 70 per anum—see Figure 1A [5–11]. Although there have been historical reviews of diamond anvil cells and high-pressure research [2,4,11–15], the growing importance of ***Laser-induced materials processing within Diamond Anvil Cells (L-DACs)*** is the motivation for this review.

L-DAC systems have yielded many scientific firsts, from establishing material equations of state and phase transitions at extreme conditions [16–19] to synthesising novel materials [20–25]. Recent examples include the synthesis of solid metallic phases of hydrogen [26,27], metallic xenon phases [28], iron-nitrogen composites [23], and binary Fe-Bi intermetallic compounds [24] (to name just a few). Laser heating allows for precise control of sample temperatures during processing at high pressures–and therefore strongly influences the resulting phases and compositions that form in situ [25,29–32]. When combined with real-time material characterisation techniques, such as X-ray diffraction (XRD), sample compositions and structures can be actively controlled.

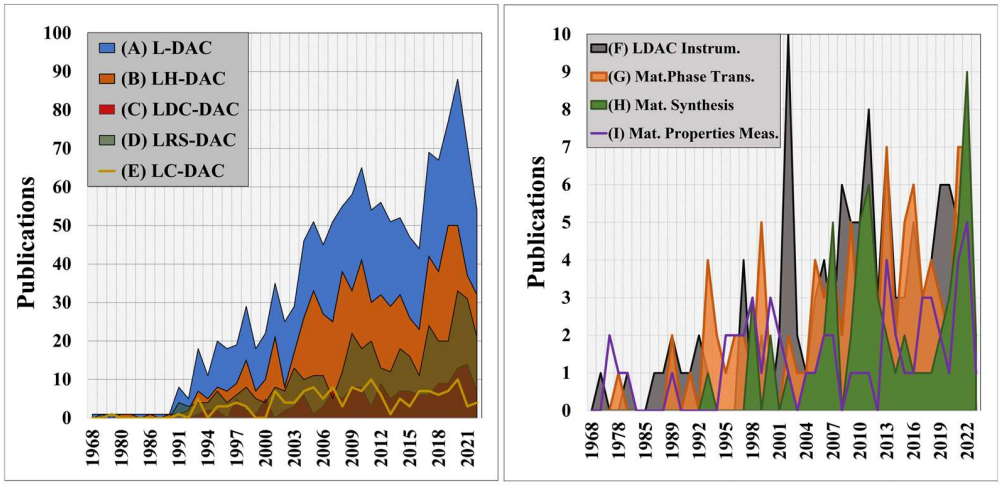

Figure 1. At left, (**A**) total annual scientific production for all L-DAC studies driven by UV-IR lasers [blue], (**B**) laser-heated diamond anvil cell (LH-DAC) articles where laser heating was employed for materials modification [orange], (**C**) laser-driven dynamic compression diamond anvil cell (LDC-DAC) experiments [red], (**D**) laser-induced reactive synthesis diamond anvil cell (LRS-DAC) articles where laser-induced reactive synthesis occurred [green], and (**E**) laser-based characterisation (LC-DAC) experiments, e.g., laser spectroscopy [yellow line]. At right, a breakdown of L-DAC articles focused on: (**F**) L-DAC instrumentation and hardware improvements [grey], (**G**) equation of state, phase transitions and phase mapping of materials [orange], (**H**) materials synthesis [green], and (**I**) material property measurements at high pressures and temperatures [purple line].

L-DAC system implementations range from "basic" laser heating and modification of samples [5,33–43] to *laser-driven dynamic compression* of materials [44–47] to *laser-induced chemical reactions* (e.g., via pyrolysis or photolysis) [25,48–51]. This article (Part I) focuses on the first of these implementations, i.e., ***laser-heated diamond anvil cells (LH-DACs)***, where a laser is focused onto a sample within a DAC to control its temperature.

In this article, we introduce the physicochemical processes that occur during laser heating at high pressures and provide a chronology of LH-DAC system development, listing important historical events. A summary of phase transformation studies to date using LH-DAC systems is given, as well as a table of materials processed with their documented process conditions of pressure, temperature, and laser source wavelengths/energies. Finally, a brief summary of complementary *laser-based characterisation methods* used frequently during LH-DAC processing is provided [7,52–61], as well as future prospects for laser-*induced* processing of materials within DACs.

Of necessity, this review is limited to laser processing within transparent anvil cells between 225 nm and 300 microns in wavelength, roughly the transmission band of diamond anvils [1,2,62]. The range of laser wavelengths used for processing in L-DAC systems to date is ~335 nm-10.6 microns [26,47,63,64]. It is also limited to pressure regimes greater than 0.01 GPa. A detailed assessment of X-ray- Deep Ultraviolet (DUV) synchrotron radiation practice and characterisation through DACs is left to future publications.

2. Methodology

This systematic review was carried out using major research databases, including the Web of Science®, ScienceDirect®, ProQuest Science®, SCOPUS®, Wiley Online Library®, IEEE Xplore®, Access Engineering®, and Google Scholar®. A preliminary literature search for the key phrase, '*diamond anvil cell*,' with no limitations on publication date, yielded over 8432 articles. This was subsequently limited by adding keywords "*laser*", "*laser-induced*", "*laser-assisted*", "*laser-heated*", "*chemical reaction*", "*shock**", "*shock-wave*", "*pressure-wave*", etc. to yield likely topical areas. For instance, adding the keyword "*laser*" filtered this list to just over 1466 publications, beginning in 1968 when the first L-DAC experiment was conducted [53].

Articles were further evaluated to ensure that the use of the word "laser" was associated with ***laser-induced processing of materials*** within a diamond anvil cell—where the laser was employed to generate a significant *modification or change in* the sample—not just as a characterisation probe. The resulting *"L-DAC"* articles were then manually classified according to their primary in situ processes. For instance, the histograms of Figure 1 were generated by arranging these categorised articles into a timeline, according to publication date.

To focus on the most impactful articles, a further criterion was applied: that the articles be cited at least 4 times; this down-selected the sampling of L-DAC papers to a final set of 290 articles, across the time span of 1968–2022. This review emphasises these 290 articles, of which the majority (71%) are related to the use of laser-heating experiments for material synthesis or modification (i.e., LH-DAC experiments). This article set was subsequently analysed using the Biblioshiny© analysis tool (from Bibliometrics) to obtain key statistical and demographics data [65]. Figure 2 displays the 12 most-cited authors and articles, as well as the 12 most used keywords, together with their relationships. It is clear that laser heating and X-ray diffraction feature prominently as important processing and characterisation techniques, while geophysical and equation-of-state (EOS) experiments dominate the applications of the published L-DAC works. The five most cited authors were Prakapenka [66], Ohishi [67], Meng [64], Hirose [67], and Dubrovinsky [68]. However, hundreds of authors contributed to the primary 290 articles selected for this review.

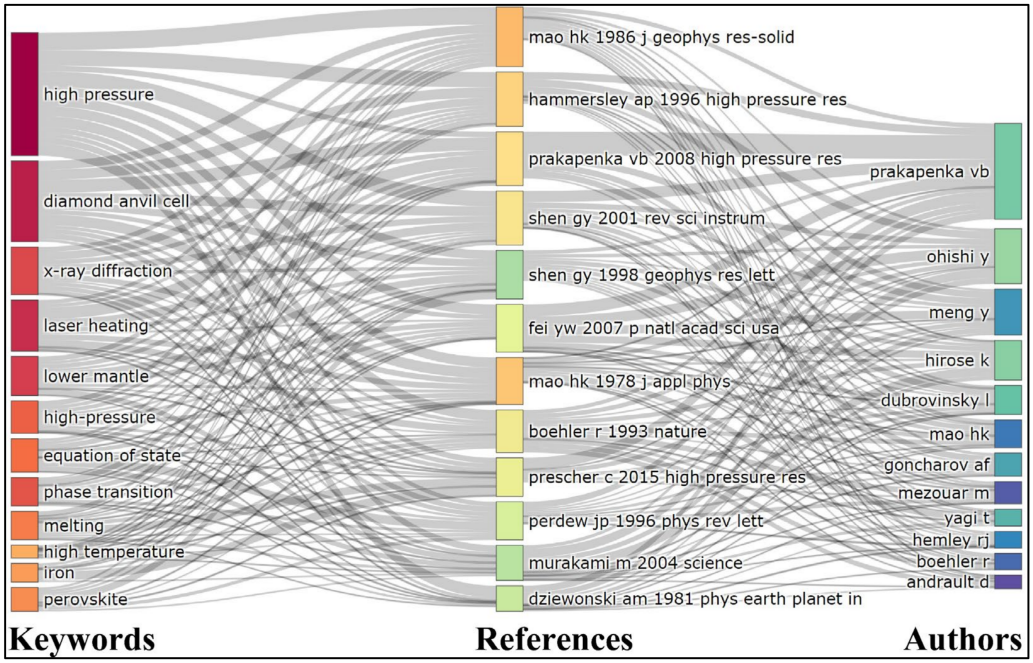

Figure 2. Three-field diagram showing relationships between the 12 most-cited authors, articles and keywords of the L-DACs works [66,69–79].

3. Overview of Laser Processing in Diamond Anvil Cells (L-DACs)

Diamond anvil cells belong to a group of devices known as opposed anvil instruments. When well-aligned and driven together, opposing diamond anvil faces generate extreme pressures on the transmitting media and sample materials trapped between them, regularly to over 300 GPa for single stage DACs [12,80]. The ultimate pressure achieved is directly proportional to the forces applied to the anvils and inversely proportional to the area of the diamond cutlets [12,81]. Where double-bevelled anvils with very small cutlets are employed, pressures greater than 400 GPa can be achieved [12]. The induced pressure can be varied dynamically through the use of pressure-driven DACs, where force is applied to at least one anvil either pneumatically or hydraulically [82–85]. DACs can also be utilised in stages to generate even greater pressures on samples; for example, Dubrovinskaia

et al. attached additional nanodiamond hemispheres into two opposing anvils to generate pressures beyond one terapascal, which they dubbed "double-DACs." [86].

In L-DAC systems, at least one anvil must be transparent, so that laser light can interact with the sample volume. Besides diamond, various highly incompressible transparent materials are occasionally used as anvils within L-DACs, e.g., cubic zirconia (ZrO_2), sapphire (Al_2O_3), and moissanite ($Si_{0.7}$–$C_{0.3}$); with these materials, pressures of up to 16.7 GPa, 25.8 GPa, and 52.1 GPa, have been generated, respectively [87–90], and depending on the samples of interest, these anvils offer some advantages for Raman and infrared spectroscopy.

However, diamond is most frequently used as an anvil material because of its impressive material properties, e.g., great compressive strength (>110 GPa) [91] and the highest thermal conductivity of any known bulk material (>2000 W/m.K) [92]. These properties allow diamond anvils to survive the extreme pressures and temperatures within an L-DAC—e.g., those induced by intense laser beams. Additionally, diamond's large bandgap energy of 5.49 eV [93] allows the anvils to be electrically insulating, such that electric currents pass through gaskets and/or samples (e.g., for resistive heating), without the anvils participating in the circuit.

Most importantly, diamond is optically transparent over an impressive wavelength band from the mid-ultraviolet (UV) to the far infrared (far-IR) [94]. This property enables experimentalists to: (1) monitor samples in situ at many wavelengths, (2) observe the alignment of anvils and samples as they are being driven, (3) employ infrared pyrometry to measure temperatures, (4) gauge chamber pressures using spectral shifts, and (5) observe the real-time structure/composition of the sample via spectroscopic methods [2]. In an L-DAC system, this optical transparency enables a wide diversity of source wavelengths to be used for heating and driving reactions [95].

Now, laser beam(s) focused into L-DAC systems can be used in several ways to process materials, e.g., through laser heating, laser-induced (shock) compression, or laser-induced chemistry. When laser heating is employed, e.g., for phase change studies, it is common practice to denote this as LH-DAC experimentation; this mode of materials processing is illustrated in Figure 3A. Here, one or two lasers (ii) are typically focused onto a sample (iii), to induce a temperature profile (T) across the sample. Often the objective in LH-DAC work is to generate a relatively flat temperature profile, while minimising any temperature gradients across the sample. In this review, sample sizes were found to range from a minimum of ≈25 to a maximum of ≈160 μm in diameter, with thicknesses ranging over 5–30 μm. For reference, typical spot sizes were in the range of 9 to >120 μm. In many cases, the laser spot sizes were large enough to be greater than their corresponding samples, which naturally provided more uniform sample heating. However, this was not true in all cases. Diamond anvils (iv) and a gasket (v) enclose (and compress) the sample through a pressure medium (ix). The LH-DAC configuration is a valuable tool for many areas of high-pressure geology, planetary science, and materials science [17,31,96–111], such as mapping P-T phase diagrams [17,101,102,105–111] or modifying materials at high pressures and high temperatures (HPHT) [37,68,112–114]. For instance, LH-DAC configurations can recreate conditions within most planetary interiors where pressures and temperatures may exceed 1 GPa and 3000 K [115].

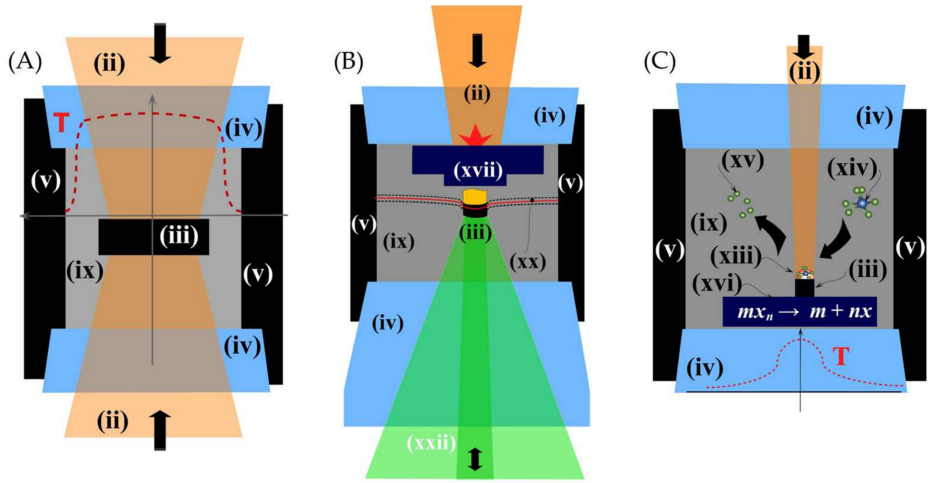

Figure 3. Illustrations of various modes of laser materials processing in L-DAC studies. (**A**) Laser-Heated Diamond Anvil Cell (LH-DAC), (**B**) Laser-driven Dynamic-Compression Diamond Anvil Cell (LDC-DAC), and (**C**) Laser Reactive Synthesis Diamond Anvil Cell (LRS-DACs) experiments. Please see article text for component descriptions.

An alternative processing mode, where the samples have already been statically compressed inside diamond anvil cells, comprises the use of a high-peak-power, short-pulsed laser beam to pass shockwaves or pressure-waves through samples, as illustrated in Figure 3B; for purposes of this review, we designate this ***Laser-driven Dynamic-Compression Diamond Anvil Cell (LDC-DAC) experimentation***. This is distinguished from *LH-DAC* experimentation by the presence of shock- or pressure-waves that significantly alter the sample's composition or structure. In this case, at least one laser beam (ii) is pulsed onto a target material (xvii), generating shock- or pressure-wave(s) (xx) that subsequently pass through the sample (iii).

Another mode of experimentation is where the laser source(s) are employed expressly to induce localised chemical reactions within diamond anvil cells. Given that the literature does not suggest any standard terminology, for purposes of this review, we designate this mode as ***Laser-induced Reactive Synthesis Diamond Anvil Cell (LRS-DAC) experimentation***—as displayed in Figure 3C. LRS-DAC experimentation is distinguished from the LH-DAC mode by the use of: (a) an intentional *chemical reaction* that changes constituents within the L-DAC chamber, (b) a chemical "precursor" to obtain a desired product, and (c) more-localised, selective heating that encourages mass transport of the precursor within the DAC.

Figure 4 provides a snapshot of the pressure-temperature (P-T) regimes that researchers have accessed using the (A) LH-DAC, (B) LDC-DAC, and (C) LRS-DAC configurations, in comparison to some geophysical and astrophysical references. Utilising *LH-DAC* configurations (orange region in Figure 4), laser-induced temperatures approaching 7500 K and static pressures of up to 377 GPa have been reached in single stage DAC's [67,116]. For comparison, using the *LDC-DAC* mode (red region) much greater dynamically induced pressures, approaching 1 TPa, have been reached [44]—and even greater pressures have been suggested as theoretically feasible (up to 100 TPa) [45]. The *LRS-DAC* configuration (green region) exhibits a similar range of temperature and pressure as the LH-DAC configuration, although most reactive synthesis studies have been caried out at temperatures well below 3000 K. Recently, the right-hand boundary of the LRS-DAC region was extended to pressures of 900 GPa using a toroidal and double stage anvil DAC [117].

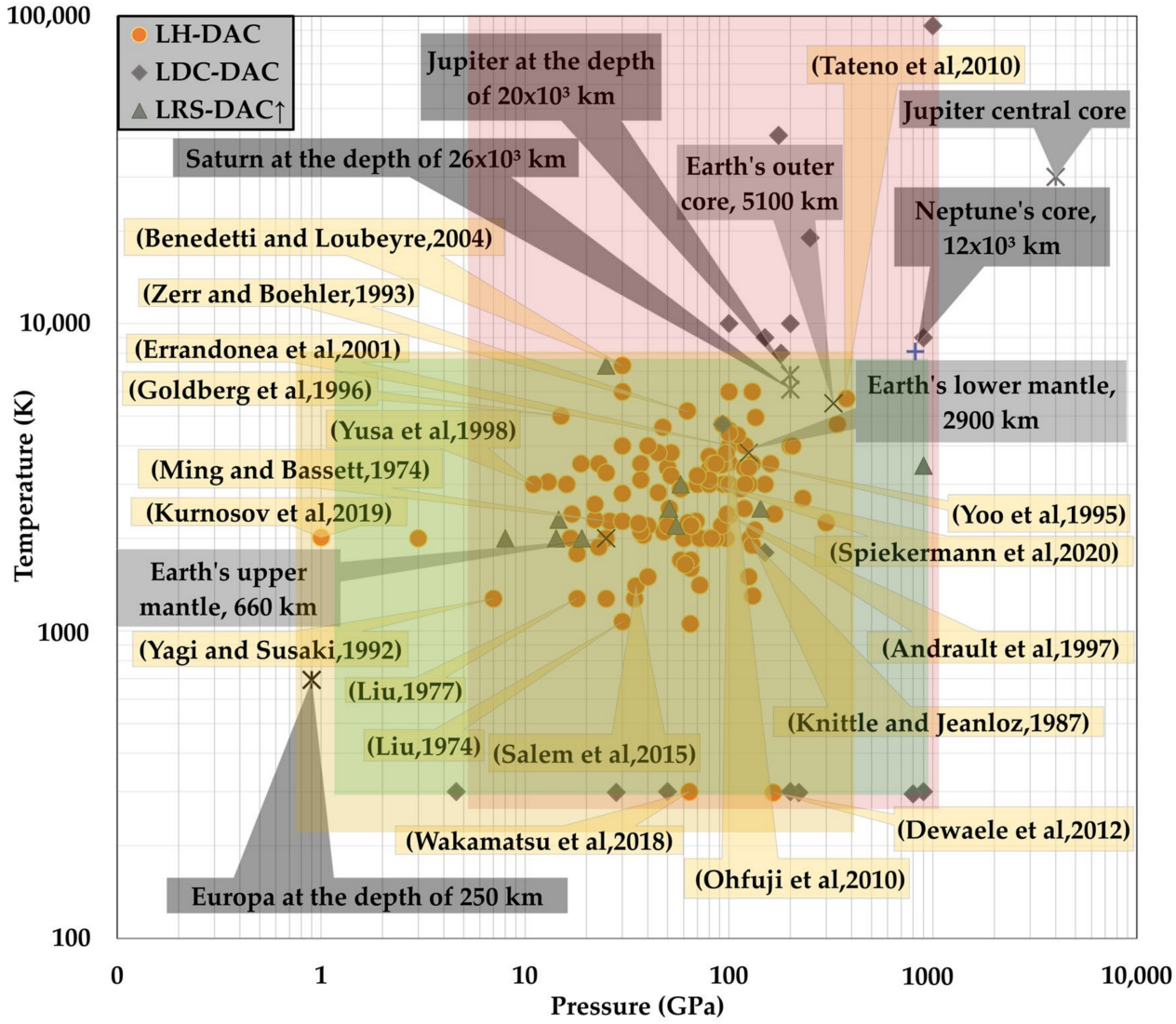

Figure 4. P-T Map of L-DAC experiments, showing regions explored by (A-Orange) LH-DAC systems [5,17,19,29,30,32,35–37,42,43,66–68,71,72,75,112–114,116,118–214], (B-Red) LDC-DAC systems [26,44,45,215–219], and (C-Green) LRS-DAC operations [3,20,23,51,220–223], in comparison to the temperature-pressure regions 250 km down in Europa's oceans [224], 660–5100 km below the Earth's surface [26,67,144], 12 $\times$ 10^3 km deep in Neptune core [225], Saturn at the depth of 26 $\times$ 10^3 km [226], and 20 $\times$ 10^3 km deep in Jupiter's atmosphere [227]. Values shown are at the peak pressures and temperatures provided in the respective references.

Now, where the laser sources are chiefly used to *characterise* materials inside diamond anvil cells, e.g., via laser spectroscopy, we name this ***Laser-Characterisation Diamond Anvil Cell (LC-DAC) experimentation***; this is distinguished from prior experimental configurations by the lack of any laser-induced modification or processing of the sample material. Of course, L-DAC systems may be implemented as combinations of two or more of the above configurations. For example, systems conducting both LH-DAC and LC-DAC activities enable real-time monitoring of phase changes while the samples are being processed [228–231].

Within this context, this review is *Part I* in a series that reviews all L-DAC material processing activities, leaving LDC-DAC and LRS-DAC investigations to parts II and III, respectively. Part I summarises the physics behind *LH-DAC* systems (e.g., those configured akin to Figure 5A)—detailing their historical development and key materials experiments. It also recaps the development of experimental methods that underlie most LH-DAC studies,

e.g., the evolution of the diamond anvil cell and common *laser-based* characterisation techniques (like the LC-DAC system illustrated in Figure 5B).

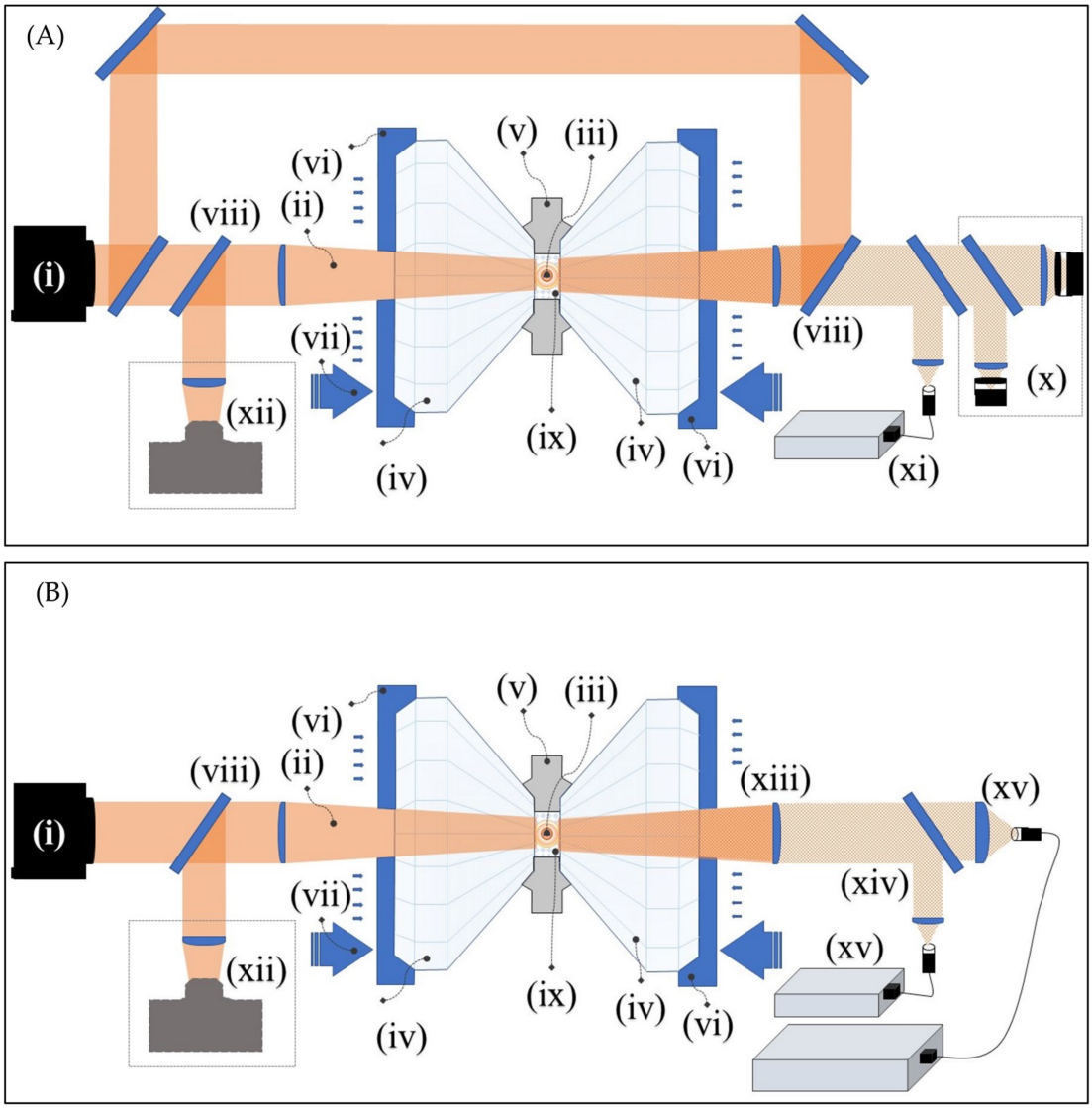

Figure 5. (**A**) Typical arrangement of Laser-Heated Diamond Anvil Cell (LH-DAC) systems for scientific/engineering experiments. (**B**) A common configuration for Laser (spectroscopic) Characterisation through Diamond Anvil Cell (LC-DAC) systems. The various elements of these systems are described in the text. Please see article text for component descriptions.

4. DACs: Fundamentals and Historical Development

The concept of using diamond, with its high compressive strength, to generate high pressures was first suggested in 1887 [232]. However, the first practical high-pressure anvil devices were developed by Bridgman in the 1930's using cantilever-arm devices to compress materials between steel or tungsten carbide plates [232]. In 1935, Bridgman further developed tungsten carbide *opposing anvil cells* [118,233]; tungsten carbide was chosen because of its high ultimate compressive strength (>2.7 GPa). In due course, these WC opposing anvils were driven by hydraulic pistons, allowing Bridgmen to ultimately achieve static pressures of over 13 GPa within thin samples of Mg_2SiO_4-Fe_2SiO_4 [15].

Improvements to Bridgman's opposing anvil apparatus were made in 1958 [234], when Tracy Hall developed *multi-anvil*, high-pressure cells, consisting of triangular WC anvils (and their driving pistons) pointed inward toward a central 3-dimensional cell—arranged in a tetrahedral geometry. This tetrahedral configuration could generate pressures over

10 GPa at temperatures of up to 3273 K, while preventing samples from easily extruding out from the cell [15]. This allowed truly three-dimensional samples to be studied, rather than just thin films.

During the same time period (1957–1958), Charlie Weir of the US National Bureau of Standards (NBS) laboratory invented the earliest *diamond anvil cells* (DACs) while attempting to transmit infrared light through a high-pressure cell with diamond windows [2]. Weir realised that one could observe the interior of the cell under a microscope while processing the sample—rather than just characterising the sample after the fact [2]. Diamond's extreme hardness and compressive strength were a clear advantage for achieving greater pressures.

In 1961, a novel DAC design with two significant improvements was developed by Sergei Stishov and Svetlana Popova of the Russian Academy of Sciences, USSR. They positioned two circular anvils across from each other with one or more concentric rings surrounding a central depression—where the sample material was located. A pressure medium was then placed within all the depressions to apply pressure to the sample [235,236]. This clever design allowed much higher pressures to be generated in the central cell, in some cases exceeding 400 GPa [237]. They named their original anvil geometry, "Chechevitsa", meaning "lentil". It was through this anvil geometry that the first ultra-dense phase of silica, "stishovite", was produced, and the design ultimately evolved into the well-known "toroidal" diamond anvil cell [235].

Meanwhile, in 1962, Van Valkenburg of Harvard University, USA, developed a method for containing liquid samples between two diamond anvils, by placing a metallic gasket with a central hole between the diamonds [238]. When compressed, the gasket sealed the liquid(s) inside [11]. The clear advantages for all DAC-related materials processing were soon realised, and the "gasket-sealed DAC" was born. The contributions of Bridgman, Hall, Weir, Stishov, Popova, and Van Valkenburg are all displayed at the left of the timeline of Figure 6, where significant events in the chronology of diamond anvil cell high-pressure techniques are exhibited.

The next innovation in DAC technologies occurred in 1970 with the development of the "Kawai-type" multi-anvil DAC; this was developed by Naoto Kawai and Shoichi Endo of Osaka University in Japan and consists of a series of split spheres, placed one inside another [239]. As pressure is applied externally, all the concentric spheres are compressed, resulting in a reduced volume ($\Delta V/V_o$) compared to traditional DACs. This allowed pressures exceeding 30 GPa to be readily attained.

In 1993, Bassett et al. also developed the first *hydrothermal diamond anvil cell* (H-DAC), designed specifically for investigating hydrothermal reactions in water-based solutions [240]. It is distinguished by resistive heaters on both the lower and upper anvils that could be precisely controlled, as well as the introduction of fluids around the gasket chamber, e.g., for sample heating/cooling. Their first H-DAC yielded pressures of $\leq$2.5 GPa with temperatures of up to 1473 K [240]—or down to 83 K with liquid nitrogen surrounding the sample.

More recently, in 2007, Evans et al. at Lawrence Livermore National Laboratory, USA, developed the *dynamic diamond anvil cell* (d-DAC), where a gas-driven platen allows the sample pressure to be changed rapidly [84]. This design makes it possible to release the pressure after processing, allowing metastable materials to be brought to room temperature and pressure before they have time to change phase. In this case, the pressure change occurs more rapidly than the phase transition kinetics. Compression and decompression rates exceeding 500 GPa/s have been achieved with this device [84].

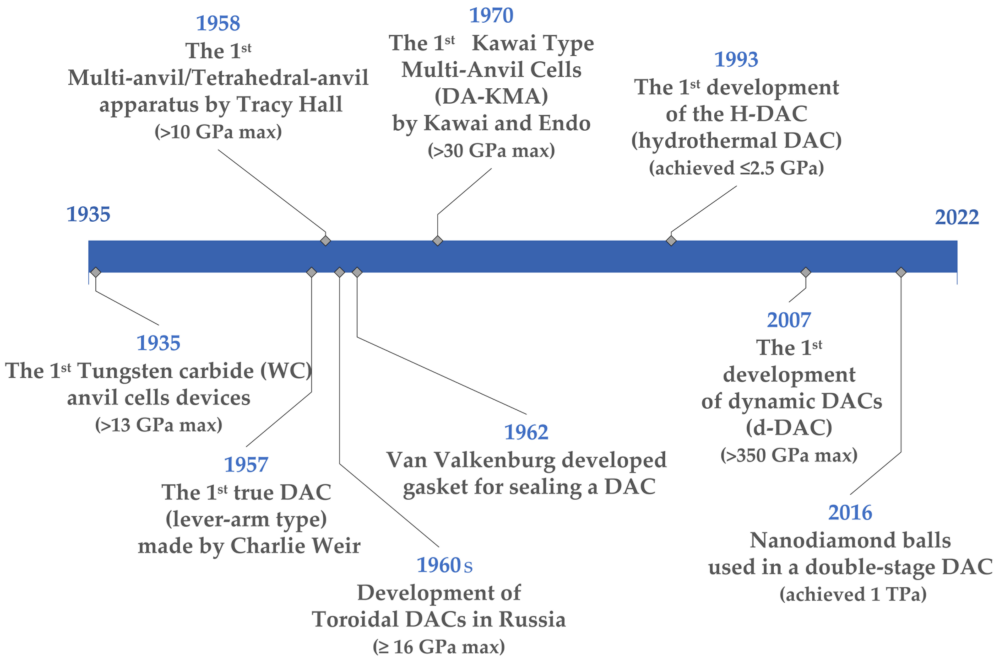

Figure 6. Chronology of Key Basic Diamond Anvil Cell (DAC) Developments/Events.

Finally, in 2016, a double-stage DAC was created, where opposing 20 μm diameter nanocrystalline diamond hemispheres were placed over the primary diamond anvils with 3 μm samples placed in-between [86]. This resulted in a record static pressure of over 1 terapascal [86].

The innovations of Kawai/Endo, Bassett et al., Evans et al., and Dubrovinskaia et al., are shown on the middle-right portion of the chronology in Figure 6. All of these important events underlie the development of modern, *L-DAC* experiments.

5. LH-DACs: Fundamentals, Historical Development, and Key Experiments

A typical LH-DAC system is illustrated in Figure 5A with a laser source (i), where at least one focused laser beam (ii) illuminates a pressured sample (iii) through transparent anvils (iv); heating is often carried out with beams illuminating both sides of the sample to obtain a more uniform temperature [4,241]. LH-DAC experiments have advantages over resistively-heated DACs in that the sample itself is heated directly, so localised extreme heating is possible without simultaneously affecting the diamond anvils or gasket chamber (v)—and sample temperatures can be measured in situ (through the anvils) [241]. In most LH-DAC configurations, significant thermal gradients may exist across extended samples, with reported values on the order of 10^7–10^9 K/m [242–246]. Such gradients can drive solid-state diffusion within samples (and within the cell overall) [6,245,247].

Additional common components of an LH-DAC system include: diamond seats (vi), a mechanism for driving the anvils (vii), laser delivery optics (viii), pressurisation media (ix), optical pyrometers (x), an optical system and spectrometer for pressure measurement (e.g., through ruby fluorescence [74]) (xi), and microscopes for general observation or process control (xii) [2,4]. As seen in Figure 4, the LH-DAC has been used to achieve laser-induced temperatures of up to ~7300 K [116]—and pressures of up to 377 GPa [67].

Key elements of an ***LC-DAC system***, shown in Figure 5B, are an excitation laser (i), sample onto which the laser is focused (iii), anvils transparent to the excitation source *and* measured spectra (iv), optics to expand and focus the laser beam(s) (viii), and optics to collimate optics (xiii) and collect emitted light (xiv) into a dedicated high-resolution spectrometer for characterisation (xv). One benefit of a DAC is that a sample can be accessed optically from both sides, so laser light can pass through a sample [2], or simply be absorbed on either side of the sample [248]. Similarly, emitted light can be accessed from either side of the DAC and be collected into two or more spectrometers through

the use of beamsplitters [136,161,180,241,249]. This allows a wide range of (spectroscopic) characterisation techniques to be carried out. For example, *UV-VIS absorption spectroscopy* (UV/VIS) [250,251], *Fourier-transform infrared spectroscopy* (FTIR) [115,252], *Raman spectroscopy* (RS) [53,220], and *frequency-domain Brilluoin scattering* (FDBS) [115,253] are all common LC-DAC spectroscopic techniques used in conjunction with DACs [52,115]. We include *laser ultrasonic* diamond anvil cell studies, sometimes abbreviated LU-DAC studies, within the LC-DAC classification [254–256]. Finally, for most studies, accurate temperature measurements across a sample are vital—these are usually carried out by analysing the black-body radiation emitted via multi-colour pyrometry or spectroscopy [54,61,257,258].

Inconsistencies in pyrometry measurements pose an ongoing challenge for all LH-DAC temperature measurements [8,166,259]. To obtain accurate temperature measurements over a wide range of temperatures, it is critical to calibrate the pyrometry-system using a black-body source, with a knowledge of the transmission of the systems optics and detector sensitivities. This is particularly true where large temperature gradients are present [260–262].

5.1. LH-DACs: Physical Processes

Frequently in LH-DAC systems, a primary objective is to maintain a uniform sample temperature for a specific time period—so that changes in phase, material properties, or crystallisation can be explored [48,120,241,263]. Lasers allow one to expose samples to extreme temperatures for extended time periods, without heating (or damaging) the entire DAC—and to achieve temperature profiles not readily obtained through resistive (external) heating [184]. For example, Zou et al. heated samples above 3500 K for 20–60 min [203]. Externally heating the entire DAC to these temperatures would have destroyed the system. Since Zou's demonstration [203], extreme laser heating for extended time periods has become quite common. In one investigation, for example, magnesiowustite and stishovite transition phases were obtained after >1 h of laser heating at >1850 $\pm$ 200 K [128].

During LH-DAC processing, the laser beam ideally heats the sample—while being transmitted through the pressurisation media and the diamond anvils. For this reason, it is important to ensure that the sample absorbs (as much as possible) the incoming light, while all other materials are transparent to the laser wavelength(s). In some cases, investigators have applied absorptive coatings or mixed-in light absorptive materials (e.g., nanoparticles) to enhance a sample's spectral absorbance, such as platinum, graphite, alumna, or lithium fluoride [30,183,193].

For continuous-wave (cw) lasers, the temperatures induced within a sample are ultimately driven by the balance of heat *absorbed* from the focused laser beam versus the heat *lost* through conduction and radiation to the surrounding environment. Diamond anvils, with their high thermal conductivity, act very effectively as heat sinks (via conduction), sandwiching the sample as illustrated in Figure 7. It is for this reason that very high incident laser powers are often reported in the LH-DAC literature; much of the power is lost through conduction to the diamond anvils.

At extreme temperatures, radiation from the heated sample can also be significant ($\sim T^4$), and this radiation can leave through the IR-transparent diamond anvils. Note that impurities in the diamond anvils may also increase laser beam losses and absorption of IR radiation (thereby directly heating the anvils), so use of colourless pure diamonds, like grades D or E, has been recommended [81].

Manga and Jeanloz have also suggested that *convective* heat transfer inside a DAC is often negligible compared to *conductive* heat transfer (or even radiative heat transfer at moderate temperatures), as they calculated the Peclet number to be less than 10^{-5} [264]; this is in part due to the diminutive L-DAC chamber volume. However, this assumption should not be taken as absolute in all experimental situations, especially where a substantial fraction of the sample volume is in a liquid state; other groups have observed very rapid convection occurring at high pressures where a large melt is present, which will undoubtedly enhance local heat transfer rates [265,266].

Of course, the laser-induced *radial* temperature distribution across a sample depends strongly on the incident laser beam profile and beam waist, ω_o. Often a Gaussian beam profile is used, as illustrated in the top plot of Figure 7. Because the induced temperature rise, ΔT, is:

$$\Delta T \sim exp\left[-a\left(\frac{r^2}{\omega_o^2}\right)\right] \quad (1)$$

Here, r is the distance from the laser axis, ω_o, is the spot waist, and a is a constant. Note that ω_o has a very strong influence on the local radiative flux—and hence ΔT [242]. So, it is exceptionally important to characterise this parameter for any LH-DAC system. Typical laser spot sizes found in the literature for LH-DAC systems are in the 30–50 µm range [40], but they were also found to be as small as 5 µm (Frereko et al.) [136] or as large as 1 mm (Kesson et al.) [147]; such values are significantly larger than the *diffraction-limited* spot sizes that could have been achieved for the laser wavelengths employed. One reason for this is that, to achieve uniform heating, it is desirable to wholly illuminate the sample (or even the entire chamber), so this often constrains the minimum spot waist employed. A more uniform radial temperature distribution can also be obtained by using flat-top profiles (or sometimes multi-mode profiles), where the samples lie within a region of relatively-constant intensity [72]. Regardless of beam profile, it is essential to characterise the actual beam intensity at the sample.

To achieve the greatest sample temperatures within a LH-DAC, it is also vital to obtain optimal alignment of the focused laser beams, so that no astigmatism is present in the optical system and (for dual beam systems) co-alignment of both beams. This is non-trivial in the confines of an LH-DAC chamber. Meng et al. developed an important alignment aid [64], which resolves some of these issues by integrating pinhead mirrors into an LH-DAC. The approach enabled precise alignment and sample temperatures of up to 6000 K with an ytterbium fibre laser [64].

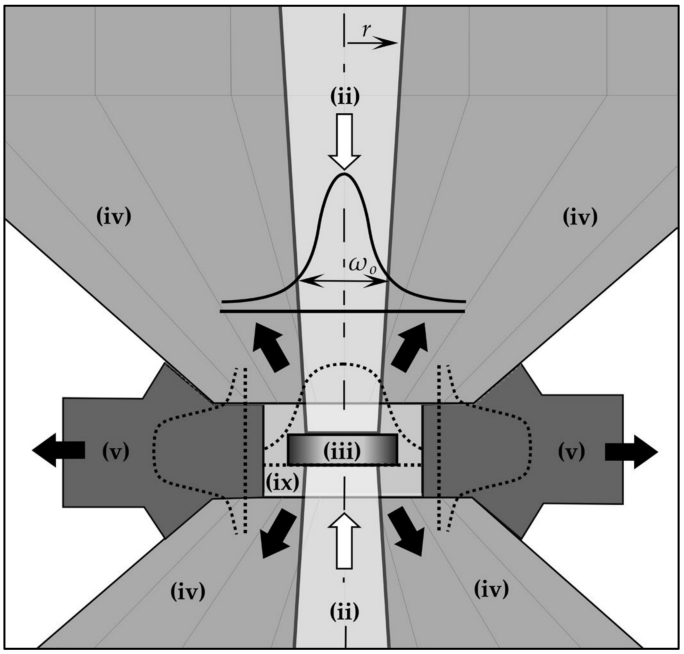

Figure 7. Schematic of Heat Transfer in an LH-DAC. With matched laser input from both sides (white arrows/beams), the resulting heat profile can be symmetric as shown (dotted graphs). Heat leaves primarily through the diamond anvils and secondarily through the gasket chamber (black arrows). Please see article text for component descriptions.

Now, as illustrated in Figure 7, a more uniform, (steady-state) temperature profile can be obtained when symmetric samples are uniformly illuminated on both sides by *cw* laser beams. Dual illumination was first implemented by Kunz et al. and Shen et al. [182,260] to eliminate the axial temperature gradients that otherwise arose in their samples [9,115]. This technique is important for many experiments where the entire sample must be heated over an extended time period—and where relatively constant temperatures are desired *axially* through the sample. Note that the temperature will still drop axially across the pressure media and approach the background temperature at/near the diamond anvils due to their extreme thermal conductivity. *Radial* heat transfer through the pressure media to the chamber gasket also occurs, but this is often less significant—especially if a poor-thermal conductor like stainless steel is used for the gasket. So, as a "rule-of-thumb", the temperature drops off rapidly close to the diamond anvils, and secondarily toward the metal gaskets.

For example, Bodea and Jeanloz observed that the induced temperatures in their LH-DAC were largely regulated by laser parameters and cooling from the diamond anvils along both the axial/radial directions [242]. They asserted that the diamond anvils remained close to ambient temperature (295 K) throughout their experiments [242]. To illustrate this, a typical temperature profile along the axis of the laser beam (with two opposing graphs) and perpendicular to the beam axis (single upright graph) are provided as dotted lines in Figure 7.

One important approach for reaching extreme temperatures is to thermally isolate the laser-heated samples from the diamond anvils [148]. For example, Ming and Bassett utilised NaCl insulation in conjunction with a graphite sample and a pulsed ruby laser [30]. Similarly, Dorfman et al. utilised NaCl insulation with synthetic olivine samples and heated them to 1900–3000 K with a fibre laser at powers up to 200 W [267]. Additionally, Shim et al. successfully employed argon as an insulating medium with an $MgSiO_3$ sample, heating it to >2500 K with an Nd:YLF laser [184]. Boehler et al. also investigated KCl and CsI insulation media around tungsten samples at temperatures of up to 3500 K [125]. Finally, Dewaele et al. reached 4950 K with alumina (Al_2O_3) coatings between the diamond anvil and the tantalum samples using argon as a pressure medium [120]. Such attempts can be improved upon by simulating the heat transfer and temperature rise. For instance, Kiefer and Duffy modelled alumina as an insulator with thicknesses up to 27 μm for silicate and oxide samples, and were (theoretically) able to reach 2200 K [148]. Additionally, Geballe and Jeanloz simulated the use of Al_2O_3 as insulation with an iron sample to produce consistent, high-pressure melting data [268].

When the illumination dwell time is sufficiently long, e.g., with cw laser sources, the thermal conductivities and heat capacities of the sample and pressurising media also influence the observed temperature profile [268]—and at very high temperatures, emissivities of the sample and pressurising media may also play important roles [116]. The utilisation of soft, highly compressible pressure media, such as noble gases, is quite common in LH-DAC systems. Such media can minimise distortion of the sample during high-pressure compression [6]. However, they can also cool the sample [94]—and (sometimes) react with the sample, which has led some researchers to avoid loading any media other than the sample (powder) itself [139,191,194]. For the reader's reference, we have listed the most commonly employed pressure media thus far in Table 1, together with their heat capacities, thermal conductivities, and initial phases at ambient conditions.

Table 1. Physical properties of common LH-DAC pressure media, including compressive strengths, thermal conductivities, and absorption coefficients at ambient conditions, 300 ± 100 K.

Material Type	Thermal Cond [W/m·k]	Heat Capacity [J/kg·K]	Phase (Form)/Prefer Laser	LH-DAC Refs.	Property Refs.
Ne	1.667	1029.9	Gas	[104,119,120,158]	[269]
Ar	1.677	520.3	Gas/CO_2	[75,104,120,126,127,132,138,158,168,180,183,184,193,195,270]	[269]
NaCl	5.4–6.49	854	Powder/YAG	[32,66,120,127,128,171,174,175,185,189,270,271]	[272]
Al_2O_3	26–34.3	753–878.6	Powder or single crystals/YAG	[119–121,144,164,193,198]	[272,273]
SiO_2	1.6–4.18	703–1000	Powder or glass pellets/YAG	[121,171,274]	[272,273]
N_2	1.4	1039	Gas	[37,112,116]	[269]
He	1.667	3115.6	Gas	[130]	[269]
MgO	18–36	877–1046	Powder/YAG	[120,131,144,198]	[272,273]
CsCl	1	317.9	Powder/YAG	[144,167,171]	[275]
KCl	6.3	690	Powder/YAG	[104,120,152,167,171,175,208]	[272]
KBr	4.8	435	Powder/YAG	[29,167]	[272]
$MgSiO_3$	5.3	811.1	dry gel	[179]	[272,276]
LiF	150, 11.3	1562	Powder/YAG	[198]	[272]
Au	317	129	foil	[211]	[272,273]

LH-DAC systems have been implemented using a wide variety of cw-laser sources, including Nd:YLF (1053 nm), Nd:YAG (1064 nm), Nd:YLF (1070 nm), and CO_2 (10.6 micron) lasers [141,151,155,176,277]. However, using continuous wave sources has several disadvantages compared to using pulsed lasers, such as (1) steady-state temperature gradient issues, (2) undesired (long-term) chemical reactions (e.g., with pressurising or insulation media), and (3) thermal diffusion which can occur across the chamber volume [64,120].

The L-DAC chamber's gasket material may also play a non-negligible role in heat transfer. For this reason, we have listed the most common LH-DAC gasket materials in Table 2, together with their compressive strengths, thermal conductivities, and heat capacities. Their typical reported gasket thicknesses are also provided. Note that rhenium and stainless steel are the most often used gaskets due to their high compressive strength and low thermal conductivity [272], but as can be seen in Table 2, tungsten, beryllium, diamond, nichrome, boron-Kapton composites, and nickel are also used. One novel gasket design by Zou et al. employed a coated 100–180 µm thick polycrystalline diamond gasket (derived from diamond powder) to examine iron oxide (FeO) in a range of 50–87 GPa up to 3500 K [203]; importantly, this design innovation provided additional internal chamber volume, thereby isolating the sample away from the diamond anvils for improved temperature control.

Table 2. Physical properties of common LH-DAC gasket materials, with their reported thickness, compressive strengths, and thermal conductivities at around room temperature ±100 K.

Material Type	Typical Gasket Thickness [µm]	Thermal Cond [W/m·k]	Heat Capacity [J/kg·K]	LH-DAC Refs.	Property Refs.
Rhenium (Re)	25–50	47.9	137	[103,105,120,127,136,139,160, 164,174,183,184,191,193,195,208, 221,229,270,274,278]	[272]
Stainless Steel	30–250	12.67	483	[29,75,138,147,148,150,170,181, 185,229,270,279]	[272]
Tungsten (W)	30–60	155	138	[140,167,179,191,229]	[92,272]
Beryllium (Be)	30	200	1825	[40,152]	[272]
Diamond	40,100	3150	520	[203,280]	[92]
Nichrome alloy (NiCr)	125	10.4–14	418–460	[42,281]	[272,273,282]
Boron-kapton composite	50	Data N/A	Data N/A	[162]	
Nickel (Ni)	200	70	450	[50]	[92]

Pulsed lasers provide a means of instantaneously heating samples in LH-DACs to extreme *peak* temperatures for short periods of time, while suppressing the *average* temperature across the L-DAC chamber. For example, Hearne et al. reached 4573 K in their LH-DAC experiment using a pulsed CO_2 laser [283]; this is a temperature that would have melted even the diamond anvils, if it had been applied across the entire cell. Long pulses (up to hundreds of ns/pulse) exhibit this effect to some degree; for example, Bassett and Weathers achieved a peak temperature of 4273 K, and Deemyad et al. achieved a temperature of 3500 K—both with minimal background heating [33,214]. However, with short pulsed lasers (<<100 ps/pulse), this effect can be taken to an extreme, where the average temperature of the chamber hardly rises above the background temperature [213]—while locally, sample peak temperatures reach thousands of degrees.

A diversity of *pulsed* lasers have been used in LH-DAC systems. Some examples include: pulsed ruby lasers at 700 nm, pulsed CO_2 lasers at 10,600 nm, yttrium lithium fluoride (YLF) lasers at 1053 nm, Nd:YAG lasers at 1064 nm, various fibre lasers (1070 nm), and femtosecond Ti/sapphire pulse lasers at 780 nm [16,30,124,155,182,195,205,206,260]. However, most pulsed lasers employed in LH-DAC systems to date have used pulse widths on the order of 1 nanosecond or longer.

5.2. LH-DAC: Historical Development

Soon after the invention of the laser in 1967, Takahashi et al. of the US National Bureau of Standards, recognised the potential of using a laser to heat samples within DACs [4], which they demonstrated a year later by converting graphite to diamond using a 694 nm ruby laser [2]. Furthermore, in 1972 Ming and Bassett performed the first temperature measurement via pyrometry with a modified Leeds and Northrup model 8632-C incandescent pyrometer at the focus of a trinocular microscope to measure a sample's temperature [4,212]. The heat source was initially a ruby (694 nm) laser, which was focused through a long-pass dichroic mirror onto the sample, so light from the sample could be observed by the pyrometer and observer.

Shortly after using the first ruby laser, Ming and Bassett upgraded their LH-DAC system with a higher-powered, 60 W cw Nd:YAG (1064 nm) laser. Using this set-up, they obtained (crude) temperature measurements of heated graphite, diamond, iron (III) oxide (Fe_2O_3), fayalite (Fe_2SiO_4), and forsterite (Mg_2SiO_4). This was the first use of an Nd:YAG laser in an LH-DAC [212]. These three initial LH-DAC developments are shown at the beginning of the timeline in Figure 8.

First used in 1991 by R. Boehler, of the Max-Planck Institute in Germany, infrared CO_2 lasers have become quite commonplace in LH-DAC experiments, as 10.6 μm transmits efficiently through diamond. Boehler et al. focused the cw infrared beam into a 100–150 micron diameter chamber at laser powers $\leq$120 W [126]. Olivine ($(Mg, Fe)_2SiO_4$), forsterite (Mg_2SiO_4), and enstatite ($MgSiO_3$) were laser-heated to >2000 K at static pressures of 10 and 25 GPa. Importantly, they were able to stabilise the laser input to <0.1% fluctuations, allowing for a constant sample temperature (within a few degrees) throughout the experiment.

Improvements in LH-DAC temperature measurement methods were made by Heinz and Jeanloz of the University of California, USA, in 1987, where they passed light directly from an LH-DAC to a spectroradiometer without the use of a beamsplitter [284]. The 1064 nm Nd:YAG laser beam was inclined at an angle to the sample, so that reflected laser light did not directly shine into the spectrometer. With this approach, they succeeded in deriving the melting point of pure uranium at pressures $\leq$45 GPa and temperatures to 2818 K and obtained radial temperature gradients in samples using a scanning slit and Abel transformations—measuring some of these to be $\sim 10^3$ K/μm. This measurement was important for ascertaining that samples can indeed be exposed to extreme temperature gradients during laser irradiation. Boehler and Heinz/Jeanloz's contributions can be found in the middle of Figure 8's timeline.

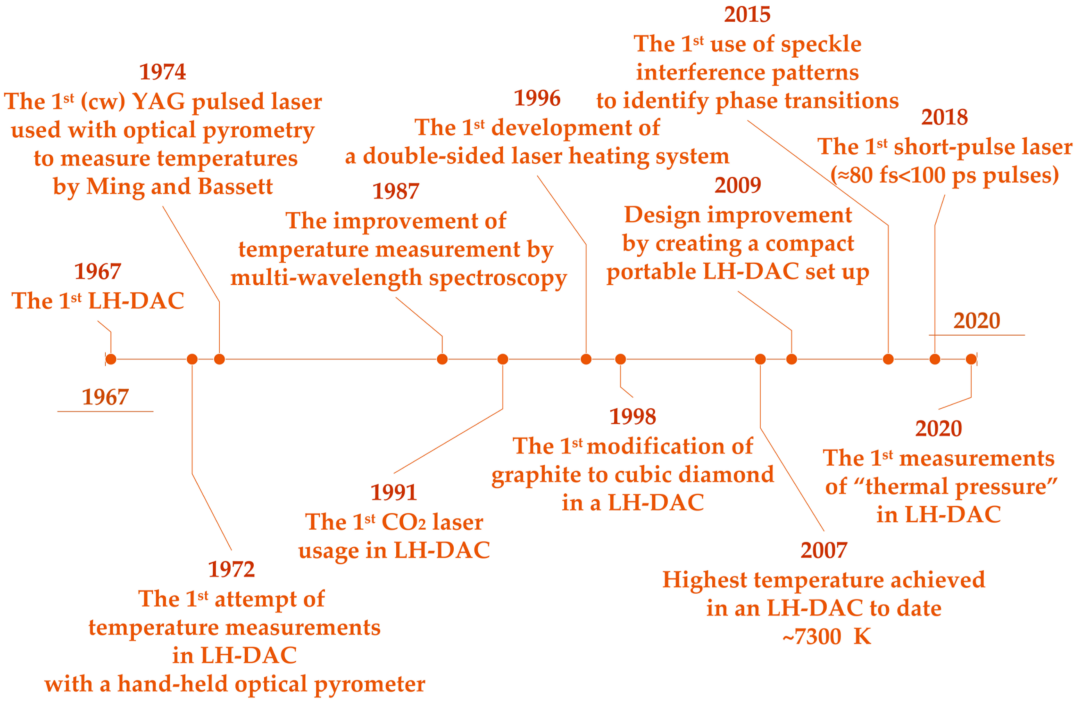

Figure 8. Chronology of Key Events in Laser-Heated Diamond Anvil Cell (LH-DAC) Development.

In 1996, Shen, Mao, and Hemley of the US Carnegie Institution for Science, revolutionised the field by introducing dual-beam illumination (to both sides of the L-DAC) and by measuring sample temperatures using an imaging spectroradiometric system that could map the temperature across a sample area. Furthermore, they utilised a multimode beam with a near-flat-top intensity profile [182]. This combination allowed for more uniform heating across large portions of the chamber, making it possible to hold samples up to 50 microns in diameter at constant temperatures, with <4% fluctuations and minimal temperature gradients. This also enabled the measurement of temperature gradients across samples. This contribution influenced many subsequent LH-DAC experiments.

With these various improvements in-place, many important materials and geo-physics experiments were carried out in the late 1990's through 2010's. One example is improved characterisation of the high-pressure graphite-to-diamond phase transition without the presence of a catalyst; in 1998, Yusa et al. [29], from National Institutes of Japan, were able to achieve consistent, high-yield conversion of graphite to the diamond phase at pressures $\geq$11.7 GPa using an LH-DAC with a single-mode CO_2 laser at 10.6 μm. The beam waist was approximately 100 μm in diameter. They held the carbon samples at temperatures of over 3000 K for 10 min. However, at lower temperatures, no conversion was observed even with higher applied pressures.

Another example is the exploration of extremely high temperatures and pressures. In 2004, Benedetti and Loubeyre of the Commissariat for Atomic Energy and Alternative Energies (CEA) [France], laser-heated elemental bromine to temperatures of ~7300 K using a double-sided LH-DAC with two 20 W Nd:YAG lasers [116]. Their objective was to create a standard for measuring temperatures at very high temperatures with bromine. As far as we know, this is the highest temperature yet sustained in an LH-DAC. The closest runner-up achieved 7000 K [130]. Realising such extreme temperatures is important for establishing high-pressure high-temperature (HPHT) phase diagrams and evaluating which phases may be present deep within the mantles or cores of planets. These two examples can be seen in the middle of the timeline in Figure 8.

Further improvements to LH-DAC experimentation occurred in 2009, when an international group from Germany, Italy, and France, developed a compact LH-DAC system that took up less than 1/2 square meter of optical breadboard space and weighed less than

20 kg [10]. The system included a DAC with ports for X-ray characterisation, double-sided laser heating, a 1070 nm Yb-doped laser with beamsplitter, spectroradiometer, automatic controls, and all opto-mechanical components. Importantly, it could be transported for rapid set-up at remote locations, such as synchrotrons. For example, Boehler et al. were able to evaluate iron's melting transition at temperatures $\leq$ 4000 K and 100 GPa pressures—while simultaneously performing X-ray absorption spectroscopy [75,107].

One clever development in 2015 by Salem et al. was the use of speckle interferometry in conjunction with an LH-DAC to quantitatively determine the onset of phase transitions, such as melting [178]. The international team, based in the Middle East and the USA, employed a secondary laser beam to generate speckle patterns which were then imaged; rapid changes in the speckle patterns indicated the likely occurrence of phase changes. This approach replaced non-objective observations by personnel with quantitative measurements by an electronic system that could respond much more accurately to phase transitions. This is especially significant for processes that employ rapid cw or pulsed laser heating—where phase changes can develop much faster than any human's response time.

Another important development in 2018 was the first use of short-pulsed lasers in an LH-DAC system with pulse widths less than 100 ps [213]. Wakamatsu et al., from Japan, demonstrated laser heating and excitation with a 30 mW femtosecond Ti:Sapphire laser beam at 780 nm and 80 MHz pulse repetition rates. Not only did they briefly heat the sample with each 80 fs (pump) pulse, but the pulses generated elastic waves from which the sound speed in the sample was determined precisely. The use of short-pulse lasers is important because materials can be processed in this manner with minimal (immediate) heat transfer to the surrounding pressure medium. Non-equilibrium processes can occur in conjunction with very rapid temperature changes—and with rapid cooling, metastable phases can form. This was also the first example of short-pulse, pump-probe acoustic spectroscopy of samples in an LH-DAC. Short-pulse pump-probe techniques allow for time-resolved imaging and characterisation of samples [285]. These LH-DAC contributions are displayed on the right-hand side of Figure 8.

Recently, the first quantitative measurements of the *thermal pressure distribution* across an LH-DAC sample were carried out by a team of researchers from the University of California and the US Advanced Light Source [259] Thermal pressure is a localised pressure that results from a sample being heated in an isochoric (constant volume) chamber (Gay-Lussac's law). Provided the surrounding material remains solid (and retains sufficient shear strength), a *pressure gradient* is generated within an LH-DAC sample—where the highest pressure is generally at the peak laser-induced temperature. In this experiment, C. E. Yen et al. generated a large thermal gradient using a 1090 nm fibre laser, heating silver iodide and olivine using the double-sided illumination method [259]. They subsequently took measurements with a fine X-ray beam at various locations across the 30 µm (FWHM) laser-heated spot and obtained the *thermal pressure* distribution; this distribution had a similar profile to that of the induced-temperature gradient. This work demonstrated that the thermal pressure could indeed remain localised—and its magnitude can be significant—as in this case, it was found to be as high as 0.1 GPa/µm. Neglecting this effect can lead to inaccurate pressure measurements.

5.3. LH-DAC: Key Experiments

Figure 9 provides an overview of 28 separate phase transformation experiments down-selected from the 206 LH-DAC-relevant articles, where melting curves were measured within LH-DACs for pure elements and binary/ternary compounds. Some of these were advanced materials of technological significance, such as diamond or gallium nitride (GaN). Others were significant for geophysical studies, such as nickel (Ni), cobalt (Co), copper (Cu), periclase (MgO), iron oxide (FeO), iron-nickel alloys (FeNi), nickel silicide (NiSi), and ferropericlase (Mg,Fe)O; in Figure 9, these are compared to contemporary estimates of the pressure-temperature curve for the Earth's mantle/core. Finally, some of these were applicable to improving high-pressure techniques, e.g., measuring melting curves

for pressure transmitting media: argon (Ar), xenon (Xe), sodium chloride (NaCl), and potassium chloride (KCl).

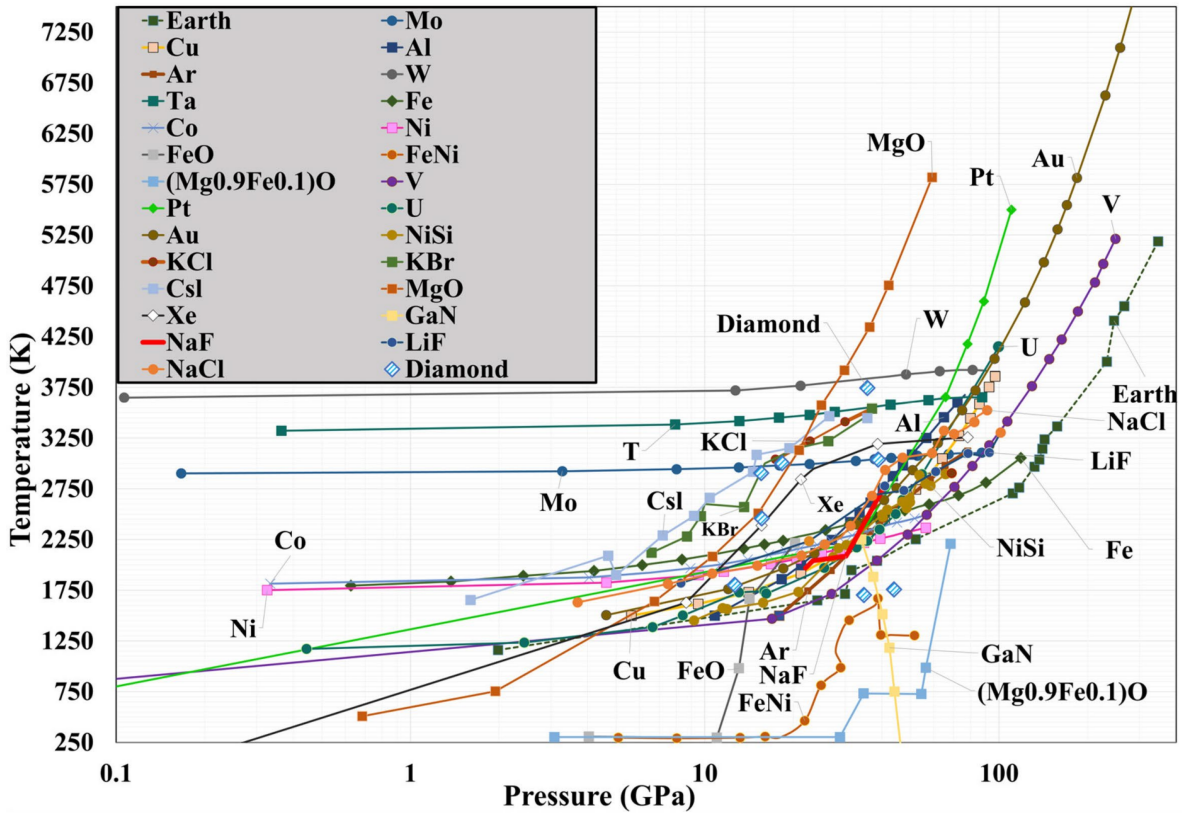

Figure 9. Example of phase transformation studies using LH-DAC systems, chosen from the selected 206 articles, showing melting curves of many elements and various binary/ternary alloys and compounds. Earth's P-T curve is shown for comparison in the mantle to core regime. Adapted from [35,38,144,159,162,173,175,196,208,241,265,286].

Among the data in Figure 9 are several noteworthy experiments that impacted their field or changed how LH-DAC studies were performed. For example, during one experiment by Miyagi et al., $(Mg_{0.9}Fe_{0.1})O$ was pressurised to 29 GPa and heated to over 2273 K, thereby simulating conditions in the mid-mantle [162]; it was discovered that deformation mechanisms of ferropericlase do not alter substantially at such extreme pressures/temperatures—useful information for modelling mid-mantle dynamics. In another example, MgO was heated through the dual illumination method with two CO_2 lasers at 10.6 microns to over 3700 K, and a melting curve was fit to the data [286]. The authors developed an improved method of determining the melting curve(s) of metals/minerals—by monitoring the temperature vs. laser power curve (observing latent heat) and through analysis of the microtexture in quenched samples. Lastly, gallium nitride was pressurised to 3 GPa and laser-heated to 2000 K by Shukla et al. without oxidation; this work demonstrated that it is possible to laser-heat a material that normally would oxidise at extreme temperatures through careful chamber and media preparation [185]. For example, the Cr-doped Al_2O_3 (ruby), ordinarily used to measure applied pressure, was isolated into a separate section of the chamber, so that oxygen could not diffuse to the sample.

For our reader's reference, Tables 3 and 4 provides a summary of the many materials/minerals that have been explored using LH-DAC methods. Table 3 focuses on industrial materials with unique and valuable properties, such as superhardness, while Table 4 summarises modification/synthesis of geological/planetary minerals. Overall, emphasis has largely been on the exploration of phase diagrams, realisation of new material phases, and developing equations of state.

Table 3. Physical processes and experiment parameters of industrial materials produced in selected LH-DAC studies.

Modified Materials	Original Form or Phase	Press [GPa]	Laser Type [nm or μm]	Laser Power/ Energy [W/J], Spots [μm], Ind. Temps [K]	Refs.
c-BC_3	BC_3	39	Nd:YAG, 1.064 μm	200 W, 2200 K	[279]
BN-NTs	*c*-BN	5.4, 8.4	CO_2, 10.6 μm	≤240 W (60 s), 80 μm, >5000 K	[37]
c-Diamond	a: Graphite, b: Graphite w/o a catalyst	a: 20 b: 30, 45	a: Ruby, 694 nm b: CO_2, 10.6 μm	a: ≤7 J/pulse (1 ms), 20–50 μm b: 2–80 W, 50 μm	a: [29,30] b: [29]
DLC, *c*-Diamond	Pyrolytic Graphite	16.5	CO_2, 10.6 μm	120 W, ≈30 μm	[151]
a-Diamond	glassy carbon	45–50	Nd:YLF, 1064 nm	90–150 μm, 1800 K	[278]
c-Si_3N_4	*β*-Si_3N_4	a: 15 b: 30	a: Nd:YLF, 1053 nm b: CO_2, 10.6 μm	a: 35W, 2200 K b: 120 W, (1–10 min), >2800 K	[112]
ϑ-TaN	ε-TaN	23.5	Yb-Fibre	100 W, 30 μm, 3500 K	[140]
η-Ta_2N_3	ε-TaN +N	9.9	Yb-Fibre	100 W (1-sided), 30 μm, ≈2000 K	[140]
csp-Ge_3N_4	$Ge_{crystal}$ +N	14	Nd:YLF, 1053 nm	cw, 55 W, >2000 K	[3]
rs-GaN	*wz*-GaN	47	Nd:YAG, 1.06 μm	300 K	[175]

c: cubic, *DLC*: diamond like carbon, *csp*: cubic spinel, *rs*: rocksalt, *wz*: wurtzite.

Table 4. Physical processes and experimental parameters of geological/planetary minerals produced in selected LH-DAC studies.

Modified Materials	Original Form or Phase	Press [GPa]	Laser Type [nm or μm]	Laser Power/Energy [W/J], Spots [μm], Ind. Temps [K]	Refs.
tP-H_2O	ice-VII	30.9	CO_2, 10.6 μm	≈30 μm	[31]
$CaCl_2$-type-SiO_2	a: SiO_2, b: *TiO_2-type*-SiO_2	a: 80–85 b: 23	a: Nd:YAG, 1.06 μm b: Nd:YAG, 1.06 μm	a: ≈36–48 min, 60 μm, 2000 K b: cw, 40 W (2X)	a: [68] b: [127]
pv-$MgSiO_3$	$MgSiO_3$	≤86	CO_2, 10.6 μm	120 W, 2700 K	[137]
opv-$MgSiO_3$	$(Ca_{0.95}\ Fe_{0.06}Mg_{0.92}\ Na_{0.02}\ Al_{0.05})Si_2O_6$	≈24	Nd:YAG, 1.06 μm	27 W, (5–10 min)	[281]
β-Mg_2SiO_4	Mg_2Si0_4	13	Ruby, 694 nm	≤7 J/pulse (1 ms), 20–50 μm	[30]
il-$MgSiO_3$ + *cpv*-$CaSiO_3$	$(Ca_{0.95}\ Fe_{0.06}Mg_{0.92}\ Na_{0.02}\ Al_{0.05})Si_2O_6$	≈23	Nd:YAG 1.06 μm	27 W, (5–10 min)	[281]
sp-Mg_2SiO_4 +*st*-SiO_2 + *cpv*-$CaSiO_3$	$(Ca_{0.95}\ Mg_{1.01})\ Si_2O_6$	≈17	Nd:YAG, 1.06 μm	(5–10 min)	[281]
ϵ-$MgAl_2O_4$	*sp*-$MgAl_2O_4$	28	Nd:YAG, 1.06 μm	cw, 1273.15 K	[32]

Table 4. *Cont.*

Modified Materials	Original Form or Phase	Press [GPa]	Laser Type [nm or μm]	Laser Power/Energy [W/J], Spots [μm], Ind. Temps [K]	Refs.
(CaFe$_2$O$_4$)-type-NaAlSiO$_4$	NaAlSiO$_4$	28	Nd:YAG, 1.06 μm	≈1273.15 K	[43]
≈*(dhcp)*-Fe	*ϵ (hcp)*-Fe	≈35–40	Nd:YAG, 1.06 μm	cw, ≤18 W, 1200–1500 K	[5]
opv-(Mg,Fe)SiO$_3$	(Mg,Fe)SiO$_3$	38	CO_2, 10.6 μm	≤120 W, 50–75 μm 1850 K	[128]
pv-(Mg$_{0.88}$Fe$_{0.12}$) SiO$_3$	(Mg$_{0.88}$Fe$_{0.12}$) SiO$_3$	127	Nd:YAG, 1.06 μm	cw, 2000 K	[113]
a: γ-Fe$_2$SiO$_4$b: 2FeO + SiO$_2$	Fe$_2$SiO$_4$	a: 4 b: 26	Ruby, 694 nm	Pulsed, ≤7 J	[30]
pv-Al-(Mg,Fe)-SiO$_3$ + *st*-SiO$_2$ + *pv*-CaSiO$_3$+ *F*	MORB	45, 80, 100	Nd:YAG, 1.06 μm	10–12 W, 0.9–1 mm	[147]
a: Brr-(Fe, Ni) $_2$P b: Abg-(Fe, Ni) $_2$P	(Fe, Ni) $_2$P	a: 2–4 b: 28.4–39	Yb:SiO$_2$ 1.06 μm	a: 200 W, 5 min, ~15 μm, ~1625 K b: 200 W, 8 min, ~15 μm, ~1675 K	[287]

c: cubic, *pv*: perovskite, *opv*: orthorhombic perovskite, *il*: ilmenite, *cpv*: cubic perovskite, *sp*: spinel, *st*: stishovite, *dhcp*: double-layer hcp, *rs*: rocksalt, *wz*: wurtzite, *csp*: cubic spinel, *tP*: tetragonal symmetry, *F*: sodic aluminous phase with Ca -ferrite structure, MORB: Mid-Ocean Ridge Basalt, Brr: barringerite, Abg: allabogdanite.

6. LC-DACs: Fundamentals and Historical Development

Laser *characterisation* plays a vital role in any LH-DAC experimentation, so a brief review of the most common ***Laser Characterisation Diamond Anvil Cell (LC-DAC)*** methods is provided here. This includes an introduction to spectroscopic *pressure* and *temperature* measurements, followed by the most wide-spread laser spectroscopy techniques.

6.1. Spectroscopic Pressure Measurements

Static pressure measurements are essential for all materials processing experiments within an L-DAC. Since the early days of LH-DAC experimentation, laser-induced fluorescence of ruby (Cr-doped Al_2O_3) has been the foremost method of pressure measurement. Static pressure inside the DAC is inferred by placing micro-scale particles/flakes of ruby within the pressure medium and then monitoring the fluorescence wavelength(s) with a high-resolution spectrometer [2,75,122,147,288,289]. At room temperature, ruby fluoresces at two prominent lines, known as the R1 and R2 lines, centred at ~694.3 nm and 692.9 nm, respectively [290]. These peak wavelengths increase linearly with pressure, and so can be used to infer pressure. For example, the R1-line peak shifts to about 701.2 nm at 20 GPa [289]. This method can be extended to measurements of over 150 GPa [290]. Doubled Nd:YAG lasers at 532 nm are frequently used as excitation sources, although 405 nm lasers also yield strong fluorescence signals [94,291].

Provided the ruby crystals are fully encapsulated by the pressure-transmitting medium, the L-DAC pressure can be estimated from the empirical relation [74]:

$$P_1 = \left(\frac{C_1}{C_2}\right)\left[\left(\frac{\lambda_1}{\lambda_o}\right)^{C_2} - 1\right] \quad (2)$$

Here, $C_1 \approx 1904$ and $C_2 \approx 5$. Of course, this expression is only accurate near room temperature; at elevated temperatures, corrections must be made for peak shifting and broadening [292–294]. Bassett recommended that ruby fluorescence be used only as a secondary pressure measurement for LH-DAC experiments [2], due to the inverse relationship between fluorescence and temperature. Additionally, Anzellini and Boccato cautioned against extrapolating pressure data beyond the calibrated range, instead recommending the use of Raman spectroscopy for pressures up to 400 GPa [241]. Other fluorescent materials, such as strontium tetraborate (SrB_4O_7), alexandrite (Al_2BeO_4), and samarium-doped yt-

trium aluminium garnet (Sm:$Y_3Al_5O_{12}$) have also been proposed as transducing materials, due to broadening of the ruby lines at high temperatures [59].

6.2. Optical Temperature Measurements by Micro-Scale Multi-Band Pyrometry

Knowing the true temperature of an L-DAC sample is essential for practically every high-pressure scientific endeavour. Obtaining direct, accurate measurements via implanted thermocouples/thermistors, however, is quite challenging—especially when micron-scale samples are selectively laser-heated within an LH-DAC, or when strong thermal gradients are present.

It is well-known that Planck's blackbody equation describes the radiation emitted from the surface of a heated material [284]; defining $I(\lambda, T)$ as the spectral intensity, T as the temperature [K], λ as the wavelength [nm], k_b as Boltzmann's constant, h as Planck's constant, and ε as the material's emissivity, Planck's equation can be represented as:

$$I(\lambda, T) = \frac{\varepsilon c_1}{\lambda^5 \left[\exp\left(\frac{c_2}{\lambda T}\right) - 1\right]} \quad (3)$$

Here, c is the speed of light, while c_1 and c_2 are the constants: $c_1 = 2hc^2$ and $c_2 = \frac{hc}{k_b}$.

Multi-band Pyrometry uses Equation (3) to measure the black-body radiation emanating from a material to estimate its temperature. By measuring two or more intensities at different wavelengths and applying them to Equation (3), it is possible to solve for the local temperature in terms of intensity and wavelength. Generally, the greater the number of discrete bands observed in the spectrum, the more accurate the temperature measurement that is made [295]. Multi-band pyrometry can be implemented in L-DAC systems by observing samples within the diamond anvil cell using a near infrared (NIR) or infrared (IR) microscope—and then detecting the emitted radiation through narrowband filters with sensitive photodetectors, e.g., avalanche photodiodes or photomultiplier tubes [296].

Significant effort has been required over the years to obtain accurate pyrometry measurements during L-DAC experiments [182,263,268]. A primary challenge is that the L-DAC samples are typically very small, and the pyrometer must collect radiation from micron-scale areas (<<1 mm^2). This means that the collected radiant flux is quite small and difficult to detect (can be <<pW); this is especially true at low to moderate temperatures, remembering that the radiation intensity is proportional to T^4 (Stephan's Law).

In addition, inaccuracies/variations in temperature measurements may result from many factors, including wavelength-dependent sample emissivities, sample surface roughness(es), optical absorption along the transmission path, and less-than-perfect alignment of the pyrometer's optics. Large temperature gradients across the detector's field of view also result in highly inaccurate measurements, as the detector "averages" the spectral intensities of the observed area.

The L-DAC literature contains many examples of multi-band pyrometry. For example, during the early development of the LH-DAC, Ming and Bassett employed optical pyrometry with YAG laser heating and measured sample temperatures in the range of 1273–1875 K. They also heated a graphite sample using a ruby laser, and estimated the sample's temperature to be 3273 K [30].

Systems that evaluate the intensity of radiation over a broad spectrum, rather than discrete wavelengths, are known as ***spectroradiometers***—and these generally offer more accurate temperature measurements [96,297]. Shen et al. developed a unique double micro-spectroradiometric system, integrated with an X-ray microbeam, for ultra high-temperature measurements [71]. Nuclear resonant inelastic X-ray scattering (NRIXS) was also used to independently verify their spectroradiometric methods [156]. Multiband pyrometry or spectroradiometric systems are now routinely used with almost all LH-DAC experiments.

6.3. Laser-based Spectroscopy and Characterisation

Laser-based spectroscopy has been used since the early days of materials processing in diamond anvil cells. The first ***infrared (IR) spectroscopy*** through a DAC was conducted in

1959 by Weir et al. when they observed infrared absorption spectra between 1–15 microns and noted the shift in calcite spectral lines to higher frequencies with increasing pressure [298]. In 1968, Brasch et al. performed the first ***Raman spectroscopy*** of samples within a DAC, using a He-Ne laser to study mercuric iodide (HgI_2) [53]. Additionally, in 1971, Block et al. of the US National Bureau of Standards (NBS) conducted the first ***fluorescence spectroscopy*** through a diamond anvil cell, allowing in situ pressures to be measured [11,288]. These seminal events are shown on the right side of the timeline in Figure 10.

Additional important events include: (1) The first ***Brillouin scattering*** measurements within a DAC were carried out by Bassett and Brody in 1977, measuring material elastic moduli [253]. (2) The first use of synchrotron radiation was conducted by Bassett et al. in 1978 to perform broad-spectrum and monochromatic ***X-ray diffraction*** [2]; this made it possible to measure a sample's structure in real-time as P-T conditions changed in the DAC. (3) The first ***laser-induced phonon spectroscopy*** (also known as impulsive stimulated light scattering) was attempted by Brown et al. in 1988—from which acoustic velocities and the densities of compressed materials could be determined (which helps to establish equations of state) [16]. In this case, they studied the density of methanol at pressures up to 6.8 GPa. (4) In 1996, Spetzler et al. made the first "microwave-induced" ***ultrasonic interferometry*** measurements in an DAC. Utilising a microwave source at 1.0 GHz (300 mm wavelength), they generated acoustic pulses separated by a specific time delay [299]; acoustic reflections from the front of the sample vs. the far side were then allowed to interfere—and the sound velocity through the sample (at high pressures) could be inferred from the amplitude of the superimposed signal. This method is analogous to a Michelson Interferometer, only using light-stimulated ultrasound. (5) Finally, the first use of laser ultrasonics was carried out by Decremps et al. in 2008, where a Ti:Sapphire laser with short, 100 fs pulses was used to generate acoustic waves at tens of GHz though compressed samples [256]. By measuring the attenuation of the resulting pico-second ultrasonic waves vs. the hydrostatic pressure in a DAC, elastic properties of sample materials could be determined. Most of these methods are still in common use for LH-DAC and other L-DAC experimental studies.

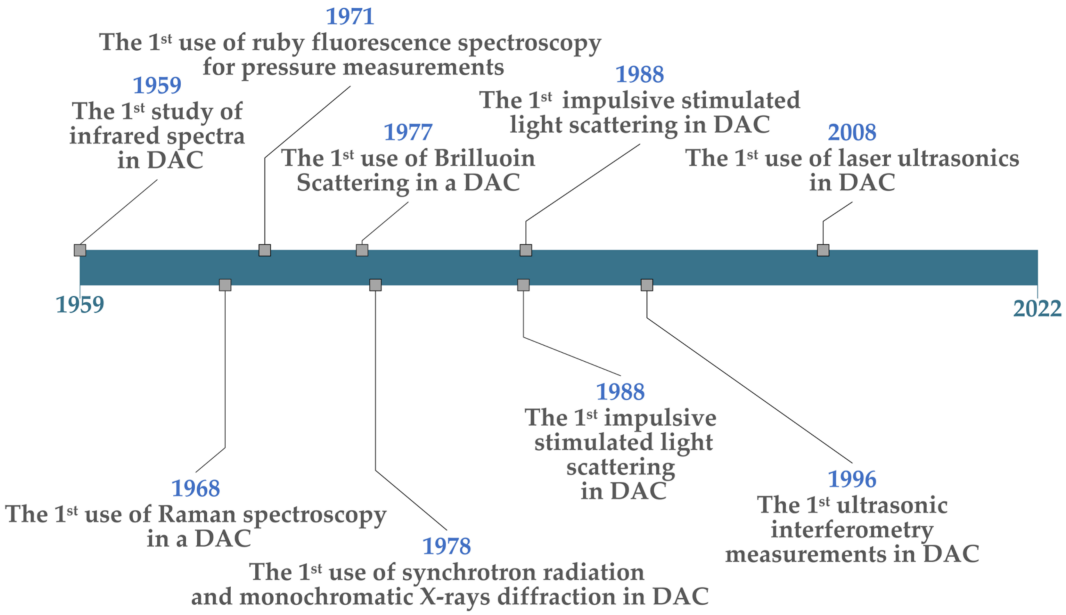

Figure 10. Chronology of Important LC-DAC developments.

7. Conclusions and Future Work

This review (part I) summarises the fundamental physics occurring within LH-DAC systems, including important heat and mass transfer processes that ultimately influence the temperature rise and material phases obtained within a DAC. It summarises the LH-DAC phase transformation studies that have been conducted over the last six decades and tabulated the many materials/minerals that have been produced by this method. In addition, related laser-based characterisation methods are introduced, e.g., Raman spectroscopy, laser-induced Brillouin scattering, and impulsive stimulated light scattering.

This work also describes the rapid advancement of the ***laser heated diamond anvil cell (LH-DAC)*** technique, where specific technical challenges have been resolved over the past six decades, e.g., generating ever-increasing pressures, obtaining accurate in situ measurements of pressure and temperature, quantitatively identifying phase/structural changes, and measuring material properties in situ. During its development, the envelope for LH-DAC studies has been extended greatly to temperatures over 7000 K and pressures beyond 300 GPa.

An examination of the LH-DAC literature suggests that historical emphasis has been placed on studying phase transformations and obtaining equations of state to better understand geological processes deep within the Earth and planetary bodies. Material property measurements have also been a primary emphasis, where studies have sought to accurately determine bulk material properties such as density, thermal conductivity, or bandgaps of materials in the compressed state; significant effort has gone into ensuring that measured phase diagrams and material properties were accurate—within the limits of the LH-DAC technology available at the time. Additionally, some complementary work has also been carried out, synthesising new or unusual materials at high pressures and temperatures, such as superhard amorphous diamond allotropes [278].

As technology continues to improve, future work will undoubtedly include more accurate measurements of material/mineral properties, verification and extrapolation of prior work to uncharted regions, and the discovery of new materials. Likely, the current P-T envelope shown in Figure 3 will be pushed even further—beyond 8000 K and 1 TPa, given improved lasers and multi-stage DACs. The advent of high-resolution high-speed digital imagers and the current proliferation of new fibre lasers and tunable excitation sources over the UV-THz regime will likely contribute to these advances. In particular, short-pulsed lasers for advanced processing and characterisation will be important for future discoveries.

It is clear, though, that the LH-DAC technique can be used for a much broader range of applications than was originally envisioned by its creators. In the last decade, many new applications have arisen, that will likely demand considerable attention. Some of these are the development of: (1) new superhard materials, (2) novel superconducting materials, and (3) photoelectric materials.

For example, recent work modifying glassy carbon to superhard sp^3-bonded amorphous diamond [278], and Shiell et al. obtaining lonsdaleite phases from glassy carbon [300], can potentially be realised, at additional purity and temperature control, via LH-DAC processing. Another example: recent investigations have shown that certain metal hydrides are high-temperature superconductors (LaH_{10} at 280 K [301,302], CaH_6 at 235 K [302,303], YH_{10} at 303 K [302,304], and H_2S at ~203 K [305]). Some of these critical temperatures (T_c) are close to room-temperature, yet their synthesis requires HPHT processing to obtain the required structure [306]. For this reason, metal hydrides (and similar compounds) are likely to be the subject of significant future investigation via LH-DACs. Additionally, here is a final example: a research team from Stanford University recently modified yellow non-perovskite δ-$CsPbI_3$ samples to the robust $CsPbI_3$ perovskite phase within a resistively heated DAC [307]. Modification to pure γ-$CsPbI_3$ is temperature dependent and is obtained by HPHT processing [307]; so this (and related materials), may potentially be generated within an LH-DAC, with improved control—and where simultaneous optical temperature measurement is available.

As Bassett stated in the 50th anniversary of the diamond anvil cell,

"*Just when I think I have heard of all the analytical methods that can be applied to samples in a diamond anvil cell, I read a paper describing yet another new method. There is no apparent end in sight. The future of diamond anvil cell research appears to be very bright indeed . . .* " [2].

Author Contributions: Conceptualisation, M.E.A. and J.L.M.; methodology, M.E.A.; investigation, M.E.A.; resources, M.E.A.; data curation, M.E.A.; writing—original draft preparation, M.E.A.; proofreading—review and editing, M.E.A., W.D.M., V.T. and J.L.M.; visualisation, M.E.A. and J.L.M.; supervision, J.L.M.; project administration, J.L.M. All authors have read and agreed to the published version of the manuscript.

Funding: Funding provided by La Trobe University Research Infrastructure Fund.

Data Availability Statement: Not applicable.

Acknowledgments: We would like to thank C. Ada and the La Trobe University Research Infrastructure Fund for their generous support of fundamental high-pressure research within the EεMC^2 Labs. This work is dedicated to our parents and grandparents, who have greatly supported us in our education and research endeavours.

Conflicts of Interest: The authors declare no conflict of interest. The funders had no role in the design of the study; in the collection, analyses, or interpretation of data; in the writing of the manuscript; or in the decision to publish the results.

References

1. Shen, G.; Mao, H.K. High-pressure studies with x-rays using diamond anvil cells. *Rep. Prog. Phys.* **2016**, *80*, 016101. [CrossRef] [PubMed]
2. Bassett, W.A. Diamond anvil cell, 50th birthday. *High Press. Res.* **2009**, *29*, 163–186. [CrossRef]
3. Serghiou, G.; Miehe, G.; Tschauner, O.; Zerr, A.; Boehler, R. Synthesis of a cubic Ge3N4 phase at high pressures and temperatures. *J. Chem. Phys.* **1999**, *111*, 4659–4662. [CrossRef]
4. Bassett, W.A. The birth and development of laser heating in diamond anvil cells. *Rev. Sci. Instrum.* **2001**, *72*, 1270–1272. [CrossRef]
5. Saxena, S.K.; Dubrovinsky, L.S.; Häggkvist, P.; Cerenius, Y.; Shen, G.; Mao, H.K. Synchrotron X-ray Study of Iron at High Pressure and Temperature. *Science* **1995**, *269*, 1703–1704. [CrossRef]
6. Andrault, D.; Fiquet, G. Synchrotron radiation and laser heating in a diamond anvil cell. *Rev. Sci. Instrum.* **2001**, *72*, 1283–1288. [CrossRef]
7. Hemley, R.J.; Mao, H.-K.; Struzhkin, V.V. Synchrotron radiation and high pressure: New light on materials under extreme conditions. *J. Synchrotron Radiat.* **2005**, *12*, 135–154. [CrossRef]
8. Kavner, A.; Panero, W.R. Temperature gradients and evaluation of thermoelastic properties in the synchrotron-based laser-heated diamond cell. *Phys. Earth Planet. Inter.* **2004**, *143–144*, 527–539. [CrossRef]
9. Duffy, T.S. Synchrotron facilities and the study of the Earth's deep interior. *Rep. Prog. Phys.* **2005**, *68*, 1811–1859. [CrossRef]
10. Boehler, R.; Musshoff, H.G.; Ditz, R.; Aquilanti, G.; Trapananti, A. Portable laser-heating stand for synchrotron applications. *Rev. Sci. Instrum.* **2009**, *80*, 045103. [CrossRef]
11. Piermarini, G.J. High pressure X-ray crystallography with the diamond cell at NIST/NBS. *J. Res. Nat. Inst. Stand. Technol.* **2001**, *106*, 889. [CrossRef]
12. O'Bannon, E.F.; Jenei, Z.; Cynn, H.; Lipp, M.J.; Jeffries, J.R. Contributed Review: Culet diameter and the achievable pressure of a diamond anvil cell: Implications for the upper pressure limit of a diamond anvil cell. *Rev. Sci. Instrum.* **2018**, *89*, 111501. [CrossRef]
13. Ren, D.; Li, H. A Review of High-Temperature and High-Pressure Experimental Apparatus Capable of Generating Differential Stress. *Front. Earth Sci.* **2022**, *10*, 852403. [CrossRef]
14. Zhao, D.; Wang, M.; Xiao, G.; Zou, B. Thinking about the Development of High-Pressure Experimental Chemistry. *J. Phys. Chem. Lett.* **2020**, *11*, 7297–7306. [CrossRef]
15. Akimoto, S.-I. High-Pressure Research in Geophysics: Past, Present and Future. In *High-Pressure Research in Mineral Physics: A Volume in Honor of Syun-iti Akimoto*; Terra Scientific Publishing Company: Tokyo, Japan, 1987; pp. 1–13.
16. Brown, J.M.; Slutsky, L.J.; Nelson, K.A.; Cheng, L.-T. Velocity of Sound and Equations of State for Methanol and Ethanol in a Diamond-Anvil Cell. *Science* **1988**, *241*, 65–67. [CrossRef]
17. Deemyad, S.; Silvera, I.F. Melting Line of Hydrogen at High Pressures. *Phys. Rev. Lett.* **2008**, *100*, 155701. [CrossRef]
18. Kavner, A.; Jeanloz, R. High-pressure melting curve of platinum. *J. Appl. Phys.* **1998**, *83*, 7553–7559. [CrossRef]
19. Kavner, A.; Jeanloz, R. The high-pressure melting curve of Allende meteorite. *Geophys. Res. Lett.* **1998**, *25*, 4161–4164. [CrossRef]

20. Yoo, C.S.; Akella, J.; Cynn, H.; Nicol, M. Direct elementary reactions of boron and nitrogen at high pressures and temperatures. *Phys. Rev. B Condens. Matter* **1997**, *56*, 140–146. [CrossRef]
21. Young, A.F.; Sanloup, C.; Gregoryanz, E.; Scandolo, S.; Hemley, R.J.; Mao, H.-K. Synthesis of Novel Transition Metal Nitrides IrN2 and OsN2. *Phys. Rev. Lett.* **2006**, *96*, 155501. [CrossRef]
22. Friedrich, A.; Winkler, B.; Bayarjargal, L.; Morgenroth, W.; Juarez-Arellano, E.A.; Milman, V.; Refson, K.; Kunz, M.; Chen, K. Novel Rhenium Nitrides. *Phys. Rev. Lett.* **2010**, *105*, 085504. [CrossRef]
23. Kumar, N.R.S.; Shekar, N.V.C.; Chandra, S.; Basu, J.; Divakar, R.; Sahu, P.C. Synthesis of novel Ru2C under high pressure–high temperature conditions. *J. Phys. Condens. Matter* **2012**, *24*, 362202. [CrossRef]
24. Walsh, J.P.S.; Freedman, D.E. High-Pressure Synthesis: A New Frontier in the Search for Next-Generation Intermetallic Compounds. *Acc. Chem. Res.* **2018**, *51*, 1315–1323. [CrossRef]
25. Aslandukova, A.; Aslandukov, A.; Yuan, L.; Laniel, D.; Khandarkhaeva, S.; Fedotenko, T.; Steinle-Neumann, G.; Glazyrin, K.; Dubrovinskaia, N.; Dubrovinsky, L. Novel High-Pressure Yttrium Carbide γ-Y4C5 Containing [C2] and Nonlinear [C3] Units with Unusually Large Formal Charges. *Phys. Rev. Lett.* **2021**, *127*, 135501. [CrossRef]
26. Brygoo, S.; Loubeyre, P.; Millot, M.; Rygg, J.R.; Celliers, P.M.; Eggert, J.H.; Jeanloz, R.; Collins, G.W. Evidence of hydrogen−helium immiscibility at Jupiter-interior conditions. *Nature* **2021**, *593*, 517–521. [CrossRef]
27. Loubeyre, P.; Occelli, F.; Dumas, P. Synchrotron infrared spectroscopic evidence of the probable transition to metal hydrogen. *Nature* **2020**, *577*, 631–635. [CrossRef]
28. Caldwell, W.A.; Nguyen, J.H.; Pfrommer, B.G.; Mauri, F.; Louie, S.G.; Jeanloz, R. Structure, bonding, and geochemistry of xenon at high pressures. *Science* **1997**, *277*, 930–933. [CrossRef]
29. Yusa, H.; Takemura, K.; Matsui, Y.; Morishima, H.; Watanabe, K.; Yamawaki, H.; Aoki, K. Direct transformation of graphite to cubic diamond observed in a laser-heated diamond anvil cell. *Appl. Phys. Lett.* **1998**, *72*, 1843–1845. [CrossRef]
30. Ming, L.C.; Bassett, W.A. Laser heating in the diamond anvil press up to 2000 °C sustained and 3000 °C pulsed at pressures up to 260 kilobars. *Rev. Sci. Instrum.* **1974**, *45*, 1115–1118. [CrossRef]
31. Grande, Z.M.; Pham, C.H.; Smith, D.; Boisvert, J.H.; Huang, C.; Smith, J.S.; Goldman, N.; Belof, J.L.; Tschauner, O.; Steffen, J.H.; et al. Pressure-driven symmetry transitions in dense H2O ice. *Phys. Rev. B Condens. Matter* **2022**, *105*, 104109. [CrossRef]
32. Liu, L.-G. A new high-pressure phase of spinel. *Earth Planet. Sci. Lett.* **1978**, *41*, 398–404. [CrossRef]
33. Bassett, W.A.; Weathers, M.S. Temperature measurement in laser heated diamond anvil cells. *Phys. B+C* **1986**, *139–140*, 900–902. [CrossRef]
34. Yang, L. How to detect melting in laser heating diamond anvil cell. *Chin. Phys. B* **2016**, *25*, 076201. [CrossRef]
35. Boehler, R.; Ross, M.; Boercker, D.B. Melting of LiF and NaCl to 1 Mbar: Systematics of Ionic Solids at Extreme Conditions. *Phys. Rev. Lett.* **1997**, *78*, 4589–4592. [CrossRef]
36. Boehler, R.; Von Bargen, N.; Chopelas, A. Melting, thermal expansion, and phase transitions of iron at high pressures. *J. Geophys. Res. Solid Earth* **1990**, *95*, 21731–21736. [CrossRef]
37. Golberg, D.; Bando, Y.; Eremets, M.; Takemura, K.; Kurashima, K.; Yusa, H. Nanotubes in boron nitride laser heated at high pressure. *Appl. Phys. Lett.* **1996**, *69*, 2045–2047. [CrossRef]
38. Jeanloz, R.; Kavner, A.; Jephcoat, A.P.; Angel, R.J.; O'Nions, R.K. Melting criteria and imaging spectroradiometry in laser-heated diamond-cell experiments. *Philos. Trans. R. Soc. Lond. Ser. A* **1996**, *354*, 1279–1305. [CrossRef]
39. Chigarev, N.; Zinin, P.; Ming, L.-C.; Amulele, G.; Bulou, A.; Gusev, V. Laser generation and detection of longitudinal and shear acoustic waves in a diamond anvil cell. *Appl. Phys. Lett.* **2008**, *93*, 181905. [CrossRef]
40. Shen, G.; Wang, L.; Ferry, R.; Mao, H.-K.; Hemley, R.J. A portable laser heating microscope for high pressure research. *J. Phys. Conf. Ser.* **2010**, *215*, 012191. [CrossRef]
41. Subramanian, N.; Struzhkin, V.V.; Goncharov, A.F.; Hemley, R.J. A virtual experiment control and data acquisition system for in situ laser heated diamond anvil cell Raman spectroscopy. *Rev. Sci. Instrum.* **2010**, *81*, 093906. [CrossRef]
42. Kim, Y.-H.; Ming, L.C.; Manghnani, M.H. High-pressure phase transformations in a natural crystalline diopside and a synthetic CaMgSi2O6 glass. *Phys. Earth Planet. Inter.* **1994**, *83*, 67–79. [CrossRef]
43. Liu, L.-G. High pressure NaAlSiO4: The first silicate calcium ferrite isotype. *Geophys. Res. Lett.* **1977**, *4*, 183–186. [CrossRef]
44. Coppari, F.; Smith, R.F.; Eggert, J.H.; Wang, J.; Rygg, J.R.; Lazicki, A.; Hawreliak, J.A.; Collins, G.W.; Duffy, T.S. Experimental evidence for a phase transition in magnesium oxide at exoplanet pressures. *Nat. Geosci.* **2013**, *6*, 926–929. [CrossRef]
45. Jeanloz, R.; Celliers, P.M.; Collins, G.W.; Eggert, J.H.; Lee, K.K.M.; McWilliams, R.S.; Brygoo, S.; Loubeyre, P. Achieving high-density states through shock-wave loading of precompressed samples. *Proc. Natl. Acad. Sci. USA* **2007**, *104*, 9172–9177. [CrossRef]
46. Eggert, J.H.; Celliers, P.M.; Hicks, D.G.; Rygg, J.R.; Collins, G.W.; Brygoo, S.; Loubeyre, P.; McWilliams, R.S.; Spaulding, D.; Jeanloz, R.; et al. Shock Experiments on Pre-Compressed Fluid Helium. *AIP Conf. Proc.* **2009**, *1161*, 26–31. [CrossRef]
47. Eggert, J.; Brygoo, S.; Loubeyre, P.; McWilliams, R.S.; Celliers, P.M.; Hicks, D.G.; Boehly, T.R.; Jeanloz, R.; Collins, G.W. Hugoniot Data for Helium in the Ionization Regime. *Phys. Rev. Lett.* **2008**, *100*, 124503. [CrossRef]
48. Yusa, H. Laser-heated diamond anvil cell system for photochemical reaction measurements. *Rev. Sci. Instrum.* **2001**, *72*, 1309–1312. [CrossRef]
49. Daviau, K.; Meng, Y.; Lee, K.K.M. SiO_2-SiC Mixtures at High Pressures and Temperatures: Implications for Planetary Bodies Containing SiC. *J. Geophys. Res. Planets* **2019**, *124*, 2294–2305. [CrossRef]

50. Goarant, F.; Guyot, F.; Peyronneau, J.; Poirier, J.-P. High-pressure and high-temperature reactions between silicates and liquid iron alloys, in the diamond anvil cell, studied by analytical electron microscopy. *J. Geophys. Res. Solid Earth* **1992**, *97*, 4477–4487. [CrossRef]
51. Sahu, P.C.; Takemura, K.; Yusa, H. Synthesis experiments on B-Sb, Ge-Sb, and Xe-Pd systems using a laser heated diamond anvil cell. *High Press. Res.* **2001**, *21*, 41–50. [CrossRef]
52. Hemley, R.J.; Bell, P.M.; Mao, H.K. Laser Techniques in High-Pressure Geophysics. *Science* **1987**, *237*, 605–612. [CrossRef] [PubMed]
53. Brasch, J.W.; Melveger, A.J.; Lippincott, E.R. Laser excited Raman spectra of samples under very high pressures. *Chem. Phys. Lett.* **1968**, *2*, 99–100. [CrossRef]
54. Shuker, P.; Melchior, A.; Assor, Y.; Belker, D.; Sterer, E. IR pyrometry in diamond anvil cell above 400K. *Rev. Sci. Instrum.* **2008**, *79*, 073908. [CrossRef] [PubMed]
55. Hrubiak, R.; Sinogeikin, S.; Rod, E.; Shen, G. The laser micro-machining system for diamond anvil cell experiments and general precision machining applications at the High Pressure Collaborative Access Team. *Rev. Sci. Instrum.* **2015**, *86*, 072202. [CrossRef] [PubMed]
56. Chang, C.-C.; Sasaki, T.; Gaida, N.A.; Niwa, K.; Hasegawa, M. Crystal and Electronic Structure of U7Te12-Type Tungsten Nitride Synthesized under High Pressure. *Inorg. Chem.* **2021**, *60*, 13278–13283. [CrossRef] [PubMed]
57. Laniel, D.; Aslandukova, A.A.; Aslandukov, A.N.; Fedotenko, T.; Chariton, S.; Glazyrin, K.; Prakapenka, V.B.; Dubrovinsky, L.S.; Dubrovinskaia, N. High-Pressure Synthesis of the β-Zn3N2 Nitride and the α-ZnN4 and β-ZnN4 Polynitrogen Compounds. *Inorg. Chem.* **2021**, *60*, 14594–14601. [CrossRef] [PubMed]
58. Prakapenka, V.B.; Holtgrewe, N.; Lobanov, S.S.; Goncharov, A.F. Structure and properties of two superionic ice phases. *Nat. Phys.* **2021**, *17*, 1233–1238. [CrossRef]
59. Yusa, H.; Yagi, T.; Arashi, H. Pressure dependence of Sm:YAG fluorescence to 50 GPa: A new calibration as a high pressure scale. *J. Appl. Phys.* **1994**, *75*, 1463–1466. [CrossRef]
60. Sui, Z.; Hu, S.; Chen, H.; Gao, C.; Su, H.; Rahman, A.; Dai, R.; Wang, Z.; Zheng, X.; Zhang, Z. Laser effects on phase transition for cubic Sb_2O_3 microcrystals under high pressure. *J. Mater. Chem. C* **2017**, *5*, 5451–5457. [CrossRef]
61. Duvaut, T. Comparison between multiwavelength infrared and visible pyrometry: Application to metals. *Infrared Phys. Technol.* **2008**, *51*, 292–299. [CrossRef]
62. Dadashev, A.; Pasternak, M.P.; Rozenberg, G.K.; Taylor, R.D. Applications of perforated diamond anvils for very high-pressure research. *Rev. Sci. Instrum.* **2001**, *72*, 2633–2637. [CrossRef]
63. Armstrong, M.R.; Crowhurst, J.C.; Bastea, S.; Zaug, J.M. Ultrafast observation of shocked states in a precompressed material. *J. Appl. Phys.* **2010**, *108*, 023511. [CrossRef]
64. Meng, Y.; Hrubiak, R.; Rod, E.; Boehler, R.; Shen, G. New developments in laser-heated diamond anvil cell with in situ synchrotron X-ray diffraction at High Pressure Collaborative Access Team. *Rev. Sci. Instrum.* **2015**, *86*, 072201. [CrossRef]
65. Aria, M.; Cuccurullo, C. bibliometrix: An R-tool for comprehensive science mapping analysis. *J. Inform.* **2017**, *11*, 959–975. [CrossRef]
66. Prakapenka, V.B.; Kubo, A.; Kuznetsov, A.; Laskin, A.; Shkurikhin, O.; Dera, P.; Rivers, M.L.; Sutton, S.R. Advanced flat top laser heating system for high pressure research at GSECARS: Application to the melting behavior of germanium. *High Press. Res.* **2008**, *28*, 225–235. [CrossRef]
67. Tateno, S.; Hirose, K.; Ohishi, Y.; Tatsumi, Y. The Structure of Iron in Earth's Inner Core. *Science* **2010**, *330*, 359–361. [CrossRef]
68. Dubrovinsky, L.S.; Saxena, S.K.; Lazor, P.; Ahuja, R.; Eriksson, O.; Wills, J.M.; Johansson, B. Experimental and theoretical identification of a new high-pressure phase of silica. *Nature* **1997**, *388*, 362–365. [CrossRef]
69. Mao, H.K.; Xu, J.; Bell, P.M. Calibration of the ruby pressure gauge to 800 kbar under quasi-hydrostatic conditions. *J. Geophys. Res. Solid Earth* **1986**, *91*, 4673–4676. [CrossRef]
70. Hammersley, A.P.; Svensson, S.O.; Hanfland, M.; Fitch, A.N.; Hausermann, D. Two-dimensional detector software: From real detector to idealised image or two-theta scan. *High Press. Res.* **1996**, *14*, 235–248. [CrossRef]
71. Shen, G.; Rivers, M.L.; Wang, Y.; Sutton, S.R. Laser heated diamond cell system at the Advanced Photon Source for in situ X-ray measurements at high pressure and temperature. *Rev. Sci. Instrum.* **2001**, *72*, 1273. [CrossRef]
72. Shen, G.; Mao, H.-K.; Hemley, R.J.; Duffy, T.S.; Rivers, M.L. Melting and crystal structure of iron at high pressures and temperatures. *Geophys. Res. Lett.* **1998**, *25*, 373–376. [CrossRef]
73. Fei, Y.; Ricolleau, A.; Frank, M.; Mibe, K.; Shen, G.; Prakapenka, V. Toward an internally consistent pressure scale. *Proc. Natl. Acad. Sci. USA* **2007**, *104*, 9182–9186. [CrossRef]
74. Mao, H.K.; Bell, P.M.; Shaner, J.W.; Steinberg, D.J. Specific volume measurements of Cu, Mo, Pd, and Ag and calibration of the ruby R1 fluorescence pressure gauge from 0.06 to 1 Mbar. *J. Appl. Phys.* **1978**, *49*, 3276–3283. [CrossRef]
75. Boehler, R. Temperatures in the Earth's core from melting-point measurements of iron at high static pressures. *Nature* **1993**, *363*, 534–536. [CrossRef]
76. Prescher, C.; Prakapenka, V.B. DIOPTAS: A program for reduction of two-dimensional X-ray diffraction data and data exploration. *High Press. Res.* **2015**, *35*, 223–230. [CrossRef]
77. Perdew, J.P.; Burke, K.; Ernzerhof, M. Generalized Gradient Approximation Made Simple. *Phys. Rev. Lett.* **1996**, *77*, 3865–3868. [CrossRef]

78. Murakami, M.; Hirose, K.; Kawamura, K.; Sata, N.; Ohishi, Y. Post-Perovskite Phase Transition in MgSiO3. *Science* **2004**, *304*, 855–858. [CrossRef]
79. Dziewonski, A.M.; Anderson, D.L. Preliminary reference Earth model. *Phys. Earth Planet. Inter.* **1981**, *25*, 297–356. [CrossRef]
80. Jayaraman, A. Ultrahigh pressures. *Rev. Sci. Instrum.* **1986**, *57*, 1013–1031. [CrossRef]
81. Soignard, E.; McMillan, P.F. An Introduction to Diamond Anvil Cells and Loading Techniques. In *High-Pressure Crystallogr*; Springer: Dordrecht, The Netherlands, 2004; pp. 81–100.
82. Webb, A.A.; Qadri, S.B. Pneumatic driver for diamond anvil cells. *Rev. Sci. Instrum.* **1982**, *53*, 1796–1797. [CrossRef]
83. Girard, E.; Fourme, R.; Ciurko, R.; Joly, J.; Bouis, F.; Legrand, P.; Jacobs, J.; Dhaussy, A.-C.; Ferrer, J.-L.; Mezouar, M.; et al. Macromolecular crystallography at high pressure with pneumatic diamond anvil cells handled by a six-axis robotic arm. *J. Appl. Crystallogr.* **2010**, *43*, 762–768. [CrossRef]
84. Evans, W.J.; Yoo, C.-S.; Lee, G.W.; Cynn, H.; Lipp, M.J.; Visbeck, K. Dynamic diamond anvil cell (dDAC): A novel device for studying the dynamic-pressure properties of materials. *Rev. Sci. Instrum.* **2007**, *78*, 073904. [CrossRef] [PubMed]
85. Dunstan, D.J.; Spain, I.L. Technology of diamond anvil high-pressure cells: I. Principles, design and construction. *J. Phys. E Sci. Instrum.* **1989**, *22*, 913–923. [CrossRef]
86. Dubrovinskaia, N.; Dubrovinsky, L.; Natalia, A.S.; Abakumov, A.; Turner, S.; Hanfland, M.; Bykova, E.; Bykov, M.; Prescher, C.; Vitali, B.P.; et al. Terapascal static pressure generation with ultrahigh yield strength nanodiamond. *Sci. Adv.* **2016**, *2*, e1600341. [CrossRef]
87. Xu, J.-A.; Mao, H.-K.; Hemley, R.J. The gem anvil cell: High-pressure behaviour of diamond and related materials. *J. Phys. Condens. Matter* **2002**, *14*, 11549–11552. [CrossRef]
88. Chen, J.; Zheng, H.; Xiao, W.; Zeng, Y. High-Temperature and High-Pressure Cubic Zirconia Anvil Cell for Raman Spectroscopy. *Appl. Spectrosc.* **2003**, *57*, 1295–1299. [CrossRef]
89. Bonetti, M.; Calmettes, P. Sapphire-anvil cell for small-angle neutron scattering measurements in large-volume liquid samples up to 530 MPa. *Rev. Sci. Instrum.* **2005**, *76*, 043903. [CrossRef]
90. Xu, J.-A.; Mao, H.-K. Moissanite: A Window for High-Pressure Experiments. *Science* **2000**, *290*, 783–785. [CrossRef]
91. Blank, V.; Popov, M.; Pivovarov, G.; Lvova, N.; Gogolinsky, K.; Reshetov, V. Ultrahard and superhard phases of fullerite C60: Comparison with diamond on hardness and wear. *Diam. Relat. Mater.* **1998**, *7*, 427–431. [CrossRef]
92. Callister, W.D. *Materials Science and Engineering*, 9th ed.; SI version; Callister, W.D., Jr., Rethwisch, D.G., Eds.; Wiley: Hoboken, NJ, USA, 2015.
93. Zaitsev, A.M. Optical Electronic Transitions. In *Optical Properties of Diamond: A Data Handbook*; Zaitsev, A.M., Ed.; Springer: Berlin/Heidelberg, Germany, 2001; pp. 125–376.
94. Bini, R.A.S.; Vincenzo. *Materials under Extreme Conditions: Molecular Crystals at High Pressure*; Imperial College Press: London, UK, 2014; Volume 1.
95. Zaitsev, A.M. Refraction. In *Optical Properties of Diamond: A Data Handbook*; Zaitsev, A.M., Ed.; Springer: Berlin/Heidelberg, Germany, 2001; pp. 1–11.
96. Subramanian, N.; Shekar, N.V.C.; Kumar, N.R.S.; Sahu, P.C. Development of laser-heated diamond anvil cell facility for synthesis of novel materials. *Curr. Sci. Assoc.* **2006**, *91*, 175–182.
97. Shekar, N.; Sahu, P.C.; Rajan, K. Laser-heated diamond-anvil cell (LHDAC) in materials science research. *J. Mater. Sci. Technol.* **2003**, *19*, 518–525.
98. Feng, W.; Yang, D.; Zhu, X.; Guo, Y.; Liao, W. Simulation of laser-generated longitudinal and shear ultrasonic waves in a diamond anvil cell by the finite element method. *J. Appl. Phys.* **2012**, *111*, 013107. [CrossRef]
99. Andrault, D.; Fiquet, G.; Itié, J.-P.; Richet, P.; Gillet, P.; Häusermann, D.; Hanfland, M. Thermal pressure in the laser-heated diamond-anvil cell: An X-ray diffraction study. *Eur. J. Miner.* **1998**, *10*, 931–940. [CrossRef]
100. Andrault, D.; Morard, G.; Bolfan-Casanova, N.; Ohtaka, O.; Fukui, H.; Arima, H.; Guignot, N.; Funakoshi, K.; Lazor, P.; Mezouar, M. Study of partial melting at high-pressure using in situ X-ray diffraction. *High Press. Res.* **2006**, *26*, 267–276. [CrossRef]
101. Anzellini, S.; Dewaele, A.; Mezouar, M.; Loubeyre, P.; Morard, G. Melting of Iron at Earth's Inner Core Boundary Based on Fast X-ray Diffraction. *Science* **2013**, *340*, 464–466. [CrossRef]
102. Anzellini, S.; Monteseguro, V.; Bandiello, E.; Dewaele, A.; Burakovsky, L.; Errandonea, D. In situ characterization of the high pressure–high temperature melting curve of platinum. *Sci. Rep.* **2019**, *9*, 13034. [CrossRef]
103. Aprilis, G.; Strohm, C.; Kupenko, I.; Linhardt, S.; Laskin, A.; Vasiukov, D.M.; Cerantola, V.; Koemets, E.G.; McCammon, C.; Kurnosov, A.; et al. Portable double-sided pulsed laser heating system for time-resolved geoscience and materials science applications. *Rev. Sci. Instrum.* **2017**, *88*, 084501. [CrossRef]
104. Aprilis, G.; Kantor, I.; Kupenko, I.; Cerantola, V.; Pakhomova, A.; Collings, I.E.; Torchio, R.; Fedotenko, T.; Chariton, S.; Bykov, M.; et al. Comparative study of the influence of pulsed and continuous wave laser heating on the mobilization of carbon and its chemical reaction with iron in a diamond anvil cell. *J. Appl. Phys.* **2019**, *125*, 095901. [CrossRef]
105. Baron, M.A.; Lord, O.T.; Myhill, R.; Thomson, A.R.; Wang, W.; Trønnes, R.G.; Walter, M.J. Experimental constraints on melting temperatures in the MgO–SiO_2 system at lower mantle pressures. *Earth Planet. Sci. Lett.* **2017**, *472*, 186–196. [CrossRef]
106. Boccato, S.; Torchio, R.; Kantor, I.; Morard, G.; Anzellini, S.; Giampaoli, R.; Briggs, R.; Smareglia, A.; Irifune, T.; Pascarelli, S. The Melting Curve of Nickel Up to 100 GPa Explored by XAS. *J. Geophys. Res. Solid Earth* **2017**, *122*, 9921–9930. [CrossRef]

107. Boehler, R. High-pressure experiments and the phase diagram of lower mantle and core materials. *Rev. Geophys.* **2000**, *38*, 221–245. [CrossRef]
108. Boehler, R.; Santamaría-Pérez, D.; Errandonea, D.; Mezouar, M. Melting, density, and anisotropy of iron at core conditions: New X-ray measurements to 150 GPa. *J. Phys. Conf. Ser.* **2008**, *121*, 022018. [CrossRef]
109. Briggs, R.; Daisenberger, D.; Lord, O.T.; Salamat, A.; Bailey, E.; Walter, M.J.; McMillan, P.F. High-pressure melting behavior of tin up to 105 GPa. *Phys. Rev. B Condens. Matter* **2017**, *95*, 054102. [CrossRef]
110. Errandonea, D. High-pressure melting curves of the transition metals Cu, Ni, Pd, and Pt. *Phys. Rev. B Condens. Matter* **2013**, *87*, 054108. [CrossRef]
111. Karandikar, A.; Boehler, R. Flash melting of tantalum in a diamond cell to 85 GPa. *Phys. Rev. B Condens. Matter* **2016**, *93*, 054107. [CrossRef]
112. Zerr, A.; Miehe, G.; Serghiou, G.; Schwarz, M.; Kroke, E.; Riedel, R.; Fueß, H.; Kroll, P.; Boehler, R. Synthesis of cubic silicon nitride. *Nature* **1999**, *400*, 340–342. [CrossRef]
113. Knittle, E.; Jeanloz, R. Synthesis and Equation of State of (Mg,Fe) SiO3 Perovskite to Over 100 Gigapascals. *Science* **1987**, *235*, 668–670. [CrossRef]
114. Liu, L.-G. Silicate perovskite from phase transformations of pyrope-garnet at high pressure and temperature. *Geophys. Res. Lett.* **1974**, *1*, 277–280. [CrossRef]
115. Mao, H.K.; Mao, W.L. *Theory and Practice: Diamond-Anvil Cells and Probes for High-P-T Mineral Physics Studies*; Elsevier Inc.: Cambridge, MA, USA, 2015; Volume 2, pp. 263–291.
116. Benedetti, L.R.; Loubeyre, P. Temperature gradients, wavelength-dependent emissivity, and accuracy of high and very-high temperatures measured in the laser-heated diamond cell. *High Press. Res.* **2004**, *24*, 423–445. [CrossRef]
117. Dubrovinsky, L.; Khandarkhaeva, S.; Fedotenko, T.; Laniel, D.; Bykov, M.; Giacobbe, C.; Bright, E.L.; Sedmak, P.; Chariton, S.; Prakapenka, V.; et al. Materials synthesis at terapascal static pressures. *Nature* **2022**, *605*, 274–278. [CrossRef]
118. Duffy, T.S.; Smith, R.F. Ultra-High Pressure Dynamic Compression of Geological Materials. *Front. Earth Sci.* **2019**, *7*, 23. [CrossRef]
119. Yoo, C.-S.; Wei, H.; Dias, R.; Shen, G.; Smith, J.; Chen, J.-Y.; Evans, W. Time-Resolved Synchrotron X-ray Diffraction on Pulse Laser Heated Iron in Diamond Anvil Cell. *J. Phys. Conf. Ser.* **2012**, *377*, 012108. [CrossRef]
120. Dewaele, A.; Mezouar, M.; Guignot, N.; Loubeyre, P. High melting points of tantalum in a laser-heated diamond anvil cell. *Phys. Rev. Lett.* **2010**, *104*, 255701. [CrossRef] [PubMed]
121. Andrault, D.; Fiquet, G.; Kunz, M.; Visocekas, F.; Häusermann, D. The Orthorhombic Structure of Iron: An in Situ Study at High-Temperature and High-Pressure. *Science* **1997**, *278*, 831–834. [CrossRef]
122. Armstrong, L.S.; Walter, M.J. Tetragonal almandine pyrope phase (TAPP): Retrograde Mg-perovskite from subducted oceanic crust? *Eur. J. Miner.* **2012**, *24*, 587–597. [CrossRef]
123. Armstrong, L.S.; Walter, M.J.; Tuff, J.R.; Lord, O.T.; Lennie, A.R.; Kleppe, A.K.; Clark, S.M. Perovskite Phase Relations in the System CaO–MgO–TiO_2–SiO_2 and Implications for Deep Mantle Lithologies. *J. Petrol.* **2012**, *53*, 611–635. [CrossRef]
124. Boehler, R. Melting of the FeFeO and the FeFeS systems at high pressure: Constraints on core temperatures. *Earth Planet. Sci. Lett.* **1992**, *111*, 217–227. [CrossRef]
125. Boehler, R.; Ross, M.; Boercker, D.B. High-pressure melting curves of alkali halides. *Phys. Rev. B Condens. Matter* **1996**, *53*, 556–563. [CrossRef]
126. Boehler, R.; Chopelas, A. A new approach to laser heating in high pressure mineral physics. *Geophys. Res. Lett.* **1991**, *18*, 1147–1150. [CrossRef]
127. Bolfan-Casanova, N.; Andrault, D.; Amiguet, E.; Guignot, N. Equation of state and post-stishovite transformation of Al-bearing silica up to 100GPa and 3000K. *Phys. Earth Planet. Inter.* **2009**, *174*, 70–77. [CrossRef]
128. Meade, C.; Mao, H.K.; Hu, J. High-Temperature Phase Transition and Dissociation of (Mg, Fe)SiO3 Perovskite at Lower Mantle Pressures. *Science* **1995**, *268*, 1743–1745. [CrossRef] [PubMed]
129. Dewaele, A.; Mezouar, M.; Guignot, N.; Loubeyre, P. Melting of lead under high pressure studied using second-scale time-resolved X-ray diffraction. *Phys. Rev. B Condens. Matter* **2007**, *76*, 144106. [CrossRef]
130. Dewaele, A.; Belonoshko, A.B.; Garbarino, G.; Occelli, F.; Bouvier, P.; Hanfland, M.; Mezouar, M. High-pressure–high-temperature equation of state of KCl and KBr. *Phys. Rev. B Condens. Matter* **2012**, *85*, 214105. [CrossRef]
131. Dobson, D.P.; Hunt, S.A.; Ahmed, J.; Lord, O.T.; Wann, E.T.H.; Santangeli, J.; Wood, I.G.; Vočadlo, L.; Walker, A.M.; Thomson, A.R.; et al. The phase diagram of NiSi under the conditions of small planetary interiors. *Phys. Earth Planet. Inter.* **2016**, *261*, 196–206. [CrossRef]
132. Errandonea, D.; Schwager, B.; Ditz, R.; Gessmann, C.; Boehler, R.; Ross, M. Systematics of transition-metal melting. *Phys. Rev. B Condens. Matter* **2001**, *63*, 132104. [CrossRef]
133. Errandonea, D.; Somayazulu, M.; Häusermann, D.; Mao, H.K. Melting of tantalum at high pressure determined by angle dispersive X-ray diffraction in a double-sided laser-heated diamond-anvil cell. *J. Phys. Condens. Matter* **2003**, *15*, 7635–7649. [CrossRef]
134. Errandonea, D.; Boehler, R.; Japel, S.; Mezouar, M.; Benedetti, L.R. Structural transformation of compressed solid Ar: An X-ray diffraction study to114 GPa. *Phys. Rev. B Condens. Matter* **2006**, *73*, 092106. [CrossRef]

135. Errandonea, D.; MacLeod, S.G.; Burakovsky, L.; Santamaria-Perez, D.; Proctor, J.E.; Cynn, H.; Mezouar, M. Melting curve and phase diagram of vanadium under high-pressure and high-temperature conditions. *Phys. Rev. B Condens. Matter* **2019**, *100*, 094111. [CrossRef]
136. Fedotenko, T.; Dubrovinsky, L.; Aprilis, G.; Koemets, E.; Snigirev, A.; Snigireva, I.; Barannikov, A.; Ershov, P.; Cova, F.; Hanfland, M.; et al. Laser heating setup for diamond anvil cells for in situ synchrotron and in house high and ultra-high pressure studies. *Rev. Sci. Instrum.* **2019**, *90*, 104501. [CrossRef]
137. Fiquet, G.; Andrault, D. Powder X-ray diffraction under extreme conditions of pressure and temperature. *J. Synchrotron Radiat.* **1999**, *6*, 81–86. [CrossRef]
138. Fiquet, G.; Andrault, D.; Itié, J.P.; Gillet, P.; Richet, P. X-ray diffraction of periclase in a laser-heated diamond-anvil cell. *Phys. Earth Planet. Inter.* **1996**, *95*, 1–17. [CrossRef]
139. Fiquet, G.; Dewaele, A.; Andrault, D.; Kunz, M.; Le Bihan, T. Thermoelastic properties and crystal structure of $MgSiO_3$ perovskite at lower mantle pressure and temperature conditions. *Geophys. Res. Lett.* **2000**, *27*, 21–24. [CrossRef]
140. Friedrich, A.; Morgenroth, W.; Bayarjargal, L.; Juarez-Arellano, E.A.; Winkler, B.; Konôpková, Z. In situ study of the high pressure high-temperature stability field of TaN and of the compressibilities of ϑ-TaN and TaON. *High Press. Res.* **2013**, *33*, 633–641. [CrossRef]
141. Heinz, D.L.; Sweeney, J.S.; Miller, P. A laser heating system that stabilizes and controls the temperature: Diamond anvil cell applications. *Rev. Sci. Instrum.* **1991**, *62*, 1568–1575. [CrossRef]
142. Hrubiak, R.; Meng, Y.; Shen, G. Microstructures define melting of molybdenum at high pressures. *Nat. Commun.* **2017**, *8*, 14562. [CrossRef]
143. Huang, X.; Li, F.; Zhou, Q.; Meng, Y.; Litasov, K.D.; Wang, X.; Liu, B.; Cui, T. Thermal equation of state of Molybdenum determined from in situ synchrotron X-ray diffraction with laser-heated diamond anvil cells. *Sci. Rep.* **2016**, *6*, 19923. [CrossRef]
144. Japel, S.; Schwager, B.; Boehler, R.; Ross, M. Melting of copper and nickel at high pressure: The role of d electrons. *Phys. Rev. Lett.* **2005**, *95*, 167801. [CrossRef]
145. Kavner, A.; Duffy, T.S. Pressure–volume–temperature paths in the laser-heated diamond anvil cell. *J. Appl. Phys.* **2001**, *89*, 1907–1914. [CrossRef]
146. Kesson, S.E.; Gerald, J.D.F. Partitioning of MgO, FeO, NiO, MnO and Cr_2O_3 between magnesian silicate perovskite and magnesiowüstite: Implications for the origin of inclusions in diamond and the composition of the lower mantle. *Earth Planet. Sci. Lett.* **1992**, *111*, 229–240. [CrossRef]
147. Kesson, S.E.; Gerald, J.D.F.; Shelley, J.M.G. Mineral chemistry and density of subducted basaltic crust at lower-mantle pressures. *Nature* **1994**, *372*, 767–769. [CrossRef]
148. Kiefer, B.; Duffy, T.S. Finite element simulations of the laser-heated diamond-anvil cell. *J. Appl. Phys.* **2005**, *97*, 114902. [CrossRef]
149. Kimura, T.; Kuwayama, Y.; Yagi, T. Melting temperatures of H_2O up to 72 GPa measured in a diamond anvil cell using CO_2 laser heating technique. *J. Chem. Phys.* **2014**, *140*, 074501. [CrossRef]
150. Ko, Y.-H.; Oh, K.H.; Kim, K.J. Installation and Operation of a Double-Sided Laser Heating System for the Synthesis of Novel Materials Under Extreme Conditions. *New Phys. Sae Mulli* **2019**, *69*, 1107–1114. [CrossRef]
151. Kumar, N.R.; Shekar, N.V.; Sekar, M.; Subramanian, N.; Mohan, P.C.; Srinivasan, M.P.; Parameswaran, P.; Sahu, P.C. Diamond and diamond-like carbon in laser heated diamond anvil cell at 16.5 GPa and above 2000 K from pyrolitic graphite. *Indian J. Pure Appl. Phys.* **2008**, *46*, 783–787.
152. Kupenko, I.; Strohm, C.; McCammon, C.; Cerantola, V.; Glazyrin, K.; Petitgirard, S.; Vasiukov, D.; Aprilis, G.; Chumakov, A.I.; Rüffer, R.; et al. Time differentiated nuclear resonance spectroscopy coupled with pulsed laser heating in diamond anvil cells. *Rev. Sci. Instrum.* **2015**, *86*, 114501. [CrossRef]
153. Lavina, B.; Dera, P.; Kim, E.; Meng, Y.; Robert, T.D.; Philippe, F.W.; Stephen, R.S.; Zhao, Y. Discovery of the recoverable high-pressure iron oxide Fe4O5. *Proc. Natl. Acad. Sci. USA* **2011**, *108*, 17281–17285. [CrossRef]
154. Lazicki, A.; Dewaele, A.; Loubeyre, P.; Mezouar, M. High-pressure–temperature phase diagram and the equation of state of beryllium. *Phys. Rev. B Condens. Matter* **2012**, *86*, 174118. [CrossRef]
155. Lin, J.-F.; Santoro, M.; Struzhkin, V.V.; Mao, H.-K.; Hemley, R.J. In situ high pressure-temperature Raman spectroscopy technique with laser-heated diamond anvil cells. *Rev. Sci. Instrum.* **2004**, *75*, 3302–3306. [CrossRef]
156. Lin, J.-F.; Sturhahn, W.; Zhao, J.; Shen, G.; Mao, H.-K.; Hemley, R.J. Absolute temperature measurement in a laser-heated diamond anvil cell. *Geophys. Res. Lett.* **2004**, *31*, L14611. [CrossRef]
157. Lin, Y.; Hu, Q.; Zhu, L.; Meng, Y. Structure and Stability of Iron Fluoride at High Pressure–Temperature and Implication for a New Reservoir of Fluorine in the Deep Earth. *Minerals* **2020**, *10*, 783. [CrossRef]
158. Liu, J.; Wang, C.; Lv, C.; Su, X.; Liu, Y.; Tang, R.; Chen, J.; Hu, Q.; Mao, H.-K.; Mao, W.L. Evidence for oxygenation of Fe-Mg oxides at mid-mantle conditions and the rise of deep oxygen. *Natl. Sci. Rev.* **2020**, *8*, nwaa096. [CrossRef] [PubMed]
159. Lord, O.T.; Wann, E.T.H.; Hunt, S.A.; Walker, A.M.; Santangeli, J.; Walter, M.J.; Dobson, D.P.; Wood, I.G.; Vočadlo, L.; Morard, G.; et al. The NiSi melting curve to 70 GPa. *Phys. Earth Planet. Inter.* **2014**, *233*, 13–23. [CrossRef]
160. Lord, O.T.; Wood, I.G.; Dobson, D.P.; Vočadlo, L.; Wang, W.; Thomson, A.R.; Wann, E.T.H.; Morard, G.; Mezouar, M.; Walter, M.J. The melting curve of Ni to 1 Mbar. *Earth Planet. Sci. Lett.* **2014**, *408*, 226–236. [CrossRef]
161. Meng, Y.; Shen, G.; Mao, H.K. Double-sided laser heating system at HPCAT for in situ X-ray diffraction at high pressures and high temperatures. *J. Phys. Condens. Matter* **2006**, *18*, S1097–S1103. [CrossRef] [PubMed]

162. Miyagi, L.; Kanitpanyacharoen, W.; Raju, S.V.; Kaercher, P.; Knight, J.; MacDowell, A.; Wenk, H.-R.; Williams, Q.; Alarcon, E.Z. Combined resistive and laser heating technique for in situ radial X-ray diffraction in the diamond anvil cell at high pressure and temperature. *Rev. Sci. Instrum.* **2013**, *84*, 025118. [CrossRef] [PubMed]
163. Nabiei, F.; Badro, J.; Boukaré, C.; Hébert, C.; Cantoni, M.; Borensztajn, S.; Wehr, N.; Gillet, P. Investigating Magma Ocean Solidification on Earth Through Laser-Heated Diamond Anvil Cell Experiments. *Geophys. Res. Lett.* **2021**, *48*, e2021GL092446. [CrossRef] [PubMed]
164. Ohfuji, H.; Irifune, T.; Okada, T.; Yagi, T.; Sumiya, H. Laser heating in nano-polycrystalline diamond anvil cell. *J. Phys. Conf. Ser.* **2010**, *215*, 012192. [CrossRef]
165. Ohtaka, O.; Andrault, D.; Bouvier, P.; Schultz, E.; Mezouar, M. Phase relations and equation of state of ZrO_2 to 100 GPa. *J. Appl. Crystallogr.* **2005**, *38*, 727–733. [CrossRef]
166. Panero, W.R.; Jeanloz, R. Temperature gradients in the laser-heated diamond anvil cell. *J. Geophys. Res. Solid Earth* **2001**, *106*, 6493–6498. [CrossRef]
167. Santamaría-Pérez, D.; Boehler, R. FeSi melting curve up to 70 GPa. *Earth Planet. Sci. Lett.* **2008**, *265*, 743–747. [CrossRef]
168. Pigott, J.S.; Reaman, D.M.; Panero, W.R. Microfabrication of controlled-geometry samples for the laser-heated diamond-anvil cell using focused ion beam technology. *Rev. Sci. Instrum.* **2011**, *82*, 115106. [CrossRef]
169. Pigott, J.S.; Velisavljevic, N.; Moss, E.K.; Draganic, N.; Jacobsen, M.K.; Meng, Y.; Hrubiak, R.; Sturtevant, B.T. Experimental melting curve of zirconium metal to 37 GPa. *J. Phys. Condens. Matter* **2020**, *32*, 355402. [CrossRef]
170. Polvani, D.A.; Meng, J.F.; Hasegawa, M.; Badding, J.V. Measurement of the thermoelectric power of very small samples at ambient and high pressures. *Rev. Sci. Instrum.* **1999**, *70*, 3586–3589. [CrossRef]
171. Prakapenka, V.B.; Shen, G.; Dubrovinsky, L.S. Carbon transport in diamond anvil cells. *High Temp. High Press.* **2003**, *35–36*, 237–249. [CrossRef]
172. Raju, S.V.; Hrubiak, R.; Drozd, V.; Saxena, S. Laser-assisted processing of Ni-Al-Co-Ti under high pressure. *Mater. Manuf. Process.* **2017**, *32*, 1606–1611. [CrossRef]
173. Ross, M.; Boehler, R.; Söderlind, P. Xenon Melting Curve to 80 GPa and 5p-d Hybridization. *Phys. Rev. Lett.* **2005**, *95*, 257801. [CrossRef]
174. Runge, C.E.; Kubo, A.; Kiefer, B.; Meng, Y.; Prakapenka, V.B.; Shen, G.; Cava, R.J.; Duffy, T.S. Equation of state of $MgGeO_3$ perovskite to 65 GPa: Comparison with the post-perovskite phase. *Phys. Chem. Miner.* **2006**, *33*, 699–709. [CrossRef]
175. Sadovyi, B.; Wierzbowska, M.; Stelmakh, S.; Boccato, S.; Gierlotka, S.; Irifune, T.; Porowski, S.; Grzegory, I. Experimental and theoretical evidence of the temperature-induced wurtzite to rocksalt phase transition in GaN under high pressure. *Phys. Rev. B Condens. Matter* **2020**, *102*, 235109. [CrossRef]
176. Saha, P.; Mukherjee, G.D. Temperature measurement in double-sided laser-heated diamond anvil cell and reaction of carbon. *Indian J. Phys.* **2021**, *95*, 621–628. [CrossRef]
177. Saha, P.; Mazumder, A.; Mukherjee, G.D. Thermal conductivity of dense hcp iron: Direct measurements using laser heated diamond anvil cell. *Geosci. Front.* **2020**, *11*, 1755–1761. [CrossRef]
178. Salem, R.; Matityahu, S.; Melchior, A.; Nikolaevsky, M.; Noked, O.; Sterer, E. Image analysis of speckle patterns as a probe of melting transitions in laser-heated diamond anvil cell experiments. *Rev. Sci. Instrum.* **2015**, *86*, 093907. [CrossRef]
179. Santamaría-Pérez, D.; Ross, M.; Errandonea, D.; Mukherjee, G.D.; Mezouar, M.; Boehler, R. X-ray diffraction measurements of Mo melting to 119 GPa and the high pressure phase diagram. *J. Chem. Phys.* **2009**, *130*, 124509. [CrossRef]
180. Schultz, E.; Mezouar, M.; Crichton, W.; Bauchau, S.; Blattmann, G.; Andrault, D.; Fiquet, G.; Boehler, R.; Rambert, N.; Sitaud, B.; et al. Double-sided laser heating system for in situ high pressure–high temperature monochromatic X-ray diffraction at the esrf. *High Press. Res.* **2005**, *25*, 71–83. [CrossRef]
181. Shen, G.; Prakapenka, V.B.; Rivers, M.L.; Sutton, S.R. Structure of Liquid Iron at Pressures up to 58 GPa. *Phys. Rev. Lett.* **2004**, *92*, 185701. [CrossRef]
182. Shen, G.; Mao, H.-K.; Hemley, R. Laser-Heated Diamond Anvil Cell Technique: Double-Sided Heating with Multimode Nd:YAG Laser. In *Advanced Materials '96 New Trends in High Pressure Research*; Akaishi, M., Ed.; The Institute: Tsukuba, Japan, 1996.
183. Shieh, S.R.; Duffy, T.S.; Shen, G. X-ray diffraction study of phase stability in SiO_2 at deep mantle conditions. *Earth Planet. Sci. Lett.* **2005**, *235*, 273–282. [CrossRef]
184. Shim, S.H.; Duffy, T.S.; Jeanloz, R.; Shen, G. Stability and crystal structure of $MgSiO_3$ perovskite to the core-mantle boundary. *Geophys. Res. Lett.* **2004**, *31*. [CrossRef]
185. Shukla, B.; Shekar, N.V.C.; Kumar, N.R.S.; Ravindran, T.R.; Sahoo, P.; Dhara, S.; Sahu, P.C. Twin chamber sample assembly in DAC and HPHT studies on GaN nano-particles. *J. Phys. Conf. Ser.* **2012**, *377*, 012014. [CrossRef]
186. Singh, A.K.; Andrault, D.; Bouvier, P. X-ray diffraction from stishovite under nonhydrostatic compression to 70 GPa: Strength and elasticity across the tetragonal→orthorhombic transition. *Phys. Earth Planet. Inter.* **2012**, *208–209*, 1–10. [CrossRef]
187. Sinmyo, R.; Hirose, K. The Soret diffusion in laser-heated diamond-anvil cell. *Phys. Earth Planet. Inter.* **2010**, *180*, 172–178. [CrossRef]
188. Sinmyo, R.; Pesce, G.; Greenberg, E.; McCammon, C.; Dubrovinsky, L. Lower mantle electrical conductivity based on measurements of Al, Fe-bearing perovskite under lower mantle conditions. *Earth Planet. Sci. Lett.* **2014**, *393*, 165–172. [CrossRef]

189. Spiekermann, G.; Kupenko, I.; Petitgirard, S.; Harder, M.; Nyrow, A.; Weis, C.; Albers, C.; Biedermann, N.; Libon, L.; Sahle, C.J.; et al. A portable on-axis laser-heating system for near-90degrees X-ray spectroscopy: Application to ferropericlase and iron silicide. *J. Synchrotron Radiat.* **2020**, *27*, 414–424. [CrossRef] [PubMed]
190. Stutzmann, V.; Dewaele, A.; Bouchet, J.; Bottin, F.; Mezouar, M. High-pressure melting curve of titanium. *Phys. Rev. B Condens. Matter* **2015**, *92*, 224110. [CrossRef]
191. Auzende, A.-L.; Gillot, J.; Coquet, A.; Hennet, L.; Ona-Nguema, G.; Bonnin, D.; Esteve, I.; Roskosz, M.; Fiquet, G. Synthesis of amorphous MgO-rich peridotitic starting material for laser-heated diamond anvil cell experiments–application to iron partitioning in the mantle. *High Press. Res.* **2011**, *31*, 199–213. [CrossRef]
192. Watanuki, T.; Shimomura, O.; Yagi, T.; Kondo, T.; Isshiki, M. Construction of laser-heated diamond anvil cell system for in situ X-ray diffraction study at SPring-8. *Rev. Sci. Instrum.* **2001**, *72*, 1289–1292. [CrossRef]
193. Weck, G.; Recoules, V.; Queyroux, J.-A.; Datchi, F.; Bouchet, J.; Ninet, S.; Garbarino, G.; Mezouar, M.; Loubeyre, P. Determination of the melting curve of gold up to 110 GPa. *Phys. Rev. B Condens. Matter* **2020**, *101*, 014106. [CrossRef]
194. Yagi, T.; Susaki, J.-I. A Laser Heating System for Diamond Anvil Using CO_2 Laser. In *High-Pressure Research: Application to Earth and Planetary Sciences*; Terra Scientific Publishing Company: Tokyo, Japan, 1992; pp. 51–54.
195. Yang, L.; Karandikar, A.; Boehler, R. Flash heating in the diamond cell: Melting curve of rhenium. *Rev. Sci. Instrum.* **2012**, *83*, 063905. [CrossRef]
196. Yoo, C.S.; Akella, J.; Moriarty, J.A. High-pressure melting temperatures of uranium: Laser-heating experiments and theoretical calculations. *Phys. Rev. B Condens. Matter* **1993**, *48*, 15529–15534. [CrossRef]
197. Yoo, C.S.; Akella, J.; Campbell, A.J.; Mao, H.K.; Hemley, R.J. Phase Diagram of Iron by in Situ X-ray Diffraction: Implications for Earth's Core. *Science* **1995**, *270*, 1473–1475. [CrossRef]
198. Yoo, C.S.; Söderlind, P.; Moriarty, J.A.; Cambell, A.J. dhcp as a possible new ϵ' phase of iron at high pressures and temperatures. *Phys. Lett. A* **1996**, *214*, 65–70. [CrossRef]
199. Zerr, A.; Boehier, R. Melting of (Mg, Fe)SiO3-Perovskite to 625 Kilobars: Indication of a High Melting Temperature in the Lower Mantle. *Science* **1993**, *262*, 553–555. [CrossRef]
200. Zhang, L.; Meng, Y.; Mao, H.-K. Unit cell determination of coexisting post-perovskite and H-phase in (Mg,Fe)SiO3 using multigrain XRD: Compositional variation across a laser heating spot at 119 GPa. *Prog. Earth Planet. Sci.* **2016**, *3*, 13. [CrossRef]
201. Zhang, D.; Jackson, J.M.; Zhao, J.; Sturhahn, W.; Alp, E.E.; Hu, M.Y.; Toellner, T.S.; Murphy, C.A.; Prakapenka, V.B. Temperature of Earth's core constrained from melting of Fe and $Fe_{0.9}Ni_{0.1}$ at high pressures. *Earth Planet. Sci. Lett.* **2016**, *447*, 72–83. [CrossRef]
202. Zinin, P.V.; Prakapenka, V.B.; Burgess, K.; Odake, S.; Chigarev, N.; Sharma, S.K. Combined laser ultrasonics, laser heating, and Raman scattering in diamond anvil cell system. *Rev. Sci. Instrum.* **2016**, *87*, 123908. [CrossRef]
203. Zou, G.; Ma, Y.; Mao, H.-K.; Hemley, R.J.; Gramsch, S.A. A diamond gasket for the laser-heated diamond anvil cell. *Rev. Sci. Instrum.* **2001**, *72*, 1298–1301. [CrossRef]
204. Weathers, M.S.; Bassett, W.A. Melting of carbon at 50 to 300 kbar. *Phys. Chem. Miner.* **1987**, *15*, 105–112. [CrossRef]
205. Huang, D.; Siebert, J.; Badro, J. High pressure partitioning behavior of Mo and W and late sulfur delivery during Earth's core formation. *Geochim. Cosmochim. Acta* **2021**, *310*, 19–31. [CrossRef]
206. Kurnosov, A.; Marquardt, H.; Dubrovinsky, L.; Potapkin, V. A waveguide-based flexible CO_2-laser heating system for diamond-anvil cell applications. *Comptes Rendus Geosci.* **2019**, *351*, 280–285. [CrossRef]
207. Chidester, B.A.; Thompson, E.C.; Fischer, R.A.; Heinz, D.L.; Prakapenka, V.B.; Meng, Y.; Campbell, A.J. Experimental thermal equation of state of B2− KCl. *Phys. Rev. B Condens. Matter* **2021**, *104*, 094107. [CrossRef]
208. Zhang, Y.; Tan, Y.; Geng, H.Y.; Salke, N.P.; Gao, Z.; Li, J.; Sekine, T.; Wang, Q.; Greenberg, E.; Prakapenka, V.B.; et al. Melting curve of vanadium up to 256 GPa: Consistency between experiments and theory. *Phys. Rev. B Condens. Matter* **2020**, *102*, 214104. [CrossRef]
209. Gaida, N.A.; Niwa, K.; Sasaki, T.; Hasegawa, M. Phase relations and thermoelasticity of magnesium silicide at high pressure and temperature. *J. Chem. Phys.* **2021**, *154*, 144701. [CrossRef]
210. Anzellini, S.; Burakovsky, L.; Turnbull, R.; Bandiello, E.; Errandonea, D. P–V–T Equation of State of Iridium Up to 80 GPa and 3100 K. *Crystals* **2021**, *11*, 452. [CrossRef]
211. Nishiyama, N.; Langer, J.; Sakai, T.; Kojima, Y.; Holzheid, A.; Gaida, N.A.; Kulik, E.; Hirao, N.; Kawaguchi, S.I.; Irifune, T.; et al. Phase relations in silicon and germanium nitrides up to 98 GPa and 2400 °C. *J. Am. Ceram. Soc.* **2019**, *102*, 2195–2202. [CrossRef]
212. Bassett, W.A.; Li-Chung, M. Disproportionation of Fe2SiO4 to 2FeO+SiO_2 at pressures up to 250kbar and temperatures up to 3000 °C. *Phys. Earth Planet. Inter.* **1972**, *6*, 154–160. [CrossRef]
213. Wakamatsu, T.; Ohta, K.; Yagi, T.; Hirose, K.; Ohishi, Y. Measurements of sound velocity in iron–nickel alloys by femtosecond laser pulses in a diamond anvil cell. *Phys. Chem. Miner.* **2018**, *45*, 589–595. [CrossRef]
214. Deemyad, S.; Sterer, E.; Barthel, C.; Rekhi, S.; Tempere, J.; Silvera, I.F. Pulsed laser heating and temperature determination in a diamond anvil cell. *Rev. Sci. Instrum.* **2005**, *76*, 125104. [CrossRef]
215. Nissim, N.; Eliezer, S.; Werdiger, M. The sound velocity throughout the P-ϱ phase-space with application to laser induced shock wave in matter precompressed by a diamond anvil cell. *J. Appl. Phys.* **2014**, *115*, 213503. [CrossRef]
216. Brygoo, S.; Millot, M.; Loubeyre, P.; Lazicki, A.E.; Hamel, S.; Qi, T.; Celliers, P.M.; Coppari, F.; Eggert, J.H.; Fratanduono, D.E.; et al. Analysis of laser shock experiments on precompressed samples using a quartz reference and application to warm dense hydrogen and helium. *J. Appl. Phys.* **2015**, *118*, 195901. [CrossRef]

217. Loubeyre, P.; Celliers, P.M.; Hicks, D.G.; Henry, E.; Dewaele, A.; Pasley, J.; Eggert, J.; Koenig, M.; Occelli, F.; Lee, K.M.; et al. Coupling static and dynamic compressions: First measurements in dense hydrogen. *High Press. Res.* **2004**, *24*, 25–31. [CrossRef]
218. Loubeyre, P.; Brygoo, S.; Eggert, J.; Celliers, P.M.; Spaulding, D.K.; Rygg, J.R.; Boehly, T.R.; Collins, G.W.; Jeanloz, R. Extended data set for the equation of state of warm dense hydrogen isotopes. *Phys. Rev. B Condens. Matter* **2012**, *86*, 144115. [CrossRef]
219. Nissim, N.; Eliezer, S.; Werdiger, M.; Perelmutter, L. Approaching the "cold curve" in laser-driven shock wave experiment of a matter precompressed by a partially perforated diamond anvil. *Laser Part. Beams* **2013**, *31*, 73–79. [CrossRef]
220. Sorb, Y.A.; Subramanian, N.; Ravindran, T.R.; Sahu, P.C. High Pressure in situ Micro-Raman Spectroscopy of Ge-Sn System Synthesized in a Laser Heated Diamond Anvil Cell. *AIP Conf. Proc.* **2011**, *1349*, 1305–1306. [CrossRef]
221. Fedotenko, T.; Dubrovinsky, L.; Khandarkhaeva, S.; Chariton, S.; Koemets, E.; Koemets, I.; Hanfland, M.; Dubrovinskaia, N. Synthesis of palladium carbides and palladium hydride in laser heated diamond anvil cells. *J. Alloy. Compd.* **2020**, *844*, 156179. [CrossRef]
222. Gréaux, S.; Andrault, D.; Gautron, L.; Bolfan-Casanova, N.; Mezouar, M. Compressibility of Ca3Al2Si3O12 perovskite up to 55 GPa. *Phys. Chem. Miner.* **2014**, *41*, 419–429. [CrossRef]
223. Zerr, A.; Serghiou, G.; Boehler, R.; Ross, M. Decomposition of alkanes at high pressures and temperatures. *High Press. Res.* **2006**, *26*, 23–32. [CrossRef]
224. Vance, S.; Harnmeijer, J.; Kimura, J.; Hussmann, H.; DeMartin, B.; Brown, J.M. Hydrothermal Systems in Small Ocean Planets. *Astrobiology* **2007**, *7*, 987–1005. [CrossRef]
225. Helled, R.; Anderson, J.D.; Podolak, M.; Schubert, G. Interior Models of Uranus and Neptune. *Astrophys. J.* **2010**, *726*, 15. [CrossRef]
226. Faure, G.; Mensing, T. *Introduction to Planetary Science*; Springer: Berlin/Heidelberg, Germany, 2007.
227. Guillot, T.; Gautier, D. 10.13-Giant Planets. In *Treatise on Geophysics*; Schubert, G., Ed.; Elsevier: Amsterdam, The Netherlands, 2007; pp. 439–464.
228. Aprilis, G.; Pakhomova, A.; Chariton, S.; Khandarkhaeva, S.; Melai, C.; Bykova, E.; Bykov, M.; Fedotenko, T.; Koemets, E.; McCammon, C.; et al. The Effect of Pulsed Laser Heating on the Stability of Ferropericlase at High Pressures. *Minerals* **2020**, *10*, 542. [CrossRef]
229. Patel, N.N.; Sunder, M.; Sharma, S.M. Laser heated diamond anvil cell facility for high temperature high pressure research: Application to material synthesis and melting studies. *Indian J. Phys.* **2018**, *92*, 1259–1269. [CrossRef]
230. Friedrich, A.; Winkler, B.; Juarez-Arellano, E.A.; Bayarjargal, L. Synthesis of Binary Transition Metal Nitrides, Carbides and Borides from the Elements in the Laser-Heated Diamond Anvil Cell and Their Structure-Property Relations. *Materials* **2011**, *4*, 1648–1692. [CrossRef]
231. Walker, D.; Lord, O.T.; Walter, M.J.; Clark, S.M. X-ray absorption contrast images of binary chemical reactions. *Chem. Geol.* **2009**, *260*, 211–220. [CrossRef]
232. Hemley, R.J.; Percy, W. Bridgman's second century. *High Press. Res.* **2010**, *30*, 581–619. [CrossRef]
233. Bridgman, P.W. Polymorphism, Principally of the Elements, up to 50,000 kg/cm^2. *Phys. Rev.* **1935**, *48*, 893–906. [CrossRef]
234. Hall, H.T. Some High-Pressure, High-Temperature Apparatus Design Considerations: Equipment for Use at 100,000 Atmospheres and 3000 °C. *Rev. Sci. Instrum.* **1958**, *29*, 267–275. [CrossRef]
235. Khvostantsev, L.G.; Slesarev, V.N.; Brazhkin, V.V. Toroid type high-pressure device: History and prospects. *High Press. Res.* **2004**, *24*, 371–383. [CrossRef]
236. Fang, J.; Bull, C.L.; Loveday, J.S.; Nelmes, R.J.; Kamenev, K.V. Strength analysis and optimisation of double-toroidal anvils for high-pressure research. *Rev. Sci. Instrum.* **2012**, *83*, 093902. [CrossRef]
237. Dewaele, A.; Loubeyre, P.; Occelli, F.; Marie, O.; Mezouar, M. Toroidal diamond anvil cell for detailed measurements under extreme static pressures. *Nat. Commun.* **2018**, *9*, 2913. [CrossRef]
238. Van Valkenburg, A. Visual Observations of High Pressure Transitions. *Rev. Sci. Instrum.* **1962**, *33*, 1462. [CrossRef]
239. Kawai, N.; Endo, S. The Generation of Ultrahigh Hydrostatic Pressures by a Split Sphere Apparatus. *Rev. Sci. Instrum.* **1970**, *41*, 1178–1181. [CrossRef]
240. Bassett, W.A.; Shen, A.H.; Bucknum, M.; Chou, I.M. A new diamond anvil cell for hydrothermal studies to 2.5 GPa and from −190 to 1200 °C. *Rev. Sci. Instrum.* **1993**, *64*, 2340–2345. [CrossRef]
241. Anzellini, S.; Boccato, S. A Practical Review of the Laser-Heated Diamond Anvil Cell for University Laboratories and Synchrotron Applications. *Crystals* **2020**, *10*, 459. [CrossRef]
242. Bodea, S.; Jeanloz, R. Model calculations of the temperature distribution in the laser-heated diamond cell. *J. Appl. Phys.* **1989**, *65*, 4688–4692. [CrossRef]
243. Williams, Q.; Knittle, E.; Jeanloz, R. The high-pressure melting curve of iron: A technical discussion. *J. Geophys. Res. Solid Earth* **1991**, *96*, 2171–2184. [CrossRef]
244. Manga, M.; Jeanloz, R. Axial temperature gradients in dielectric samples in the laser-heated diamond cell. *Geophys. Res. Lett.* **1996**, *23*, 1845–1848. [CrossRef]
245. Kavner, A.; Nugent, C. Precise measurements of radial temperature gradients in the laser-heated diamond anvil cell. *Rev. Sci. Instrum.* **2008**, *79*, 024902. [CrossRef]
246. Lord, O.T.; Wang, W. MIRRORS: A MATLAB®GUI for temperature measurement by multispectral imaging radiometry. *Rev. Sci. Instrum.* **2018**, *89*, 104903. [CrossRef]

247. Campbell, A.J. Measurement of temperature distributions across laser heated samples by multispectral imaging radiometry. *Rev. Sci. Instrum.* **2008**, *79*, 015108. [CrossRef]
248. Eremets, M.I. *High Pressure Experimental Methods*; Oxford University Press: Oxford, UK, 1996.
249. Caldwell, W.A.; Kunz, M.; Celestre, R.S.; Domning, E.E.; Walter, M.J.; Walker, D.; Glossinger, J.; MacDowell, A.A.; Padmore, H.A.; Jeanloz, R.; et al. Laser-heated diamond anvil cell at the advanced light source beamline 12.2.2. *Nucl. Instrum. Methods Phys. Res. Sect. A* **2007**, *582*, 221–225. [CrossRef]
250. Hébert, P.; Saint-Amans, C. Study of the laser-induced decomposition of energetic materials at static high-pressure by time-resolved absorption spectroscopy. *J. Phys. Conf. Ser.* **2014**, *500*, 022002. [CrossRef]
251. Goncharov, A.F.; Struzhkin, V.V.; Jacobsen, S.D. Reduced Radiative Conductivity of Low-Spin (Mg,Fe)O in the Lower Mantle. *Science* **2006**, *312*, 1205–1208. [CrossRef]
252. Hemley, R.J.; Goncharov, A.F.; Lu, R.; Struzhkin, V.V.; Li, M.; Mao, H.K. High-pressure synchrotron infrared spectroscopy at the national synchrotron light source. *Nuovo Cim. Soc. Ital. Fis. D* **1998**, *20*, 539–551. [CrossRef]
253. Bassett, W.A.; Brody, E.M. Brillouin Scattering: A New Way to Measure Elastic Moduli at High Pressures. In *High-Pressure Research*; Manghnani, M.H., Akimoto, S.-I., Eds.; Academic Press: Cambridge, MA, USA, 1977; pp. 519–532.
254. Chigarev, N.; Zinin, P.; Mounier, D.; Bulou, A.; Ming, L.C.; Acosta, T.; Gusev, V. Analysis of ultrasonic echoes induced by pulsed laser action on an iron film in a diamond anvil cell. *High Press. Res.* **2010**, *30*, 78–82. [CrossRef]
255. Chigarev, N.; Zinin, P.; Mounier, D.; Bulou, A.; Zerr, A.; Ming, L.C.; Gusev, V. Laser ultrasonic measurements in a diamond anvil cell on Fe and the KBr pressure medium. *J. Phys. Conf. Ser.* **2011**, *278*, 012017. [CrossRef]
256. Decremps, F.; Belliard, L.; Perrin, B.; Gauthier, M. Sound Velocity and Absorption Measurements under High Pressure Using Picosecond Ultrasonics in a Diamond Anvil Cell: Application to the Stability Study of AlPdMn. *Phys. Rev. Lett.* **2008**, *100*, 035502. [CrossRef] [PubMed]
257. Poprawski, W.; Gnutek, Z.; Radojewska, E.B.; Poprawski, R. Investigation of black body radiation with the aid of a self-made pyroelectric infrared detector. *Eur. J. Phys.* **2015**, *36*, 065025. [CrossRef]
258. Levendis, Y.A.; Estrada, K.R.; Hottel, H.C. Development of multicolor pyrometers to monitor the transient response of burning carbonaceous particles. *Rev. Sci. Instrum.* **1992**, *63*, 3608–3622. [CrossRef]
259. Yen, C.E.; Williams, Q.; Kunz, M. Thermal Pressure in the Laser-Heated Diamond Anvil Cell: A Quantitative Study and Implications for the Density Versus Mineralogy Correlation of the Mantle. *J. Geophys. Res. Solid Earth* **2020**, *125*, e2020JB020006. [CrossRef]
260. Kunz, M.; Yan, J.; Cornell, E.; Domning, E.E.; Yen, C.E.; Doran, A.; Beavers, C.M.; Treger, A.; Williams, Q.; MacDowell, A.A. Implementation and application of the peak scaling method for temperature measurement in the laser heated diamond anvil cell. *Rev. Sci. Instrum.* **2018**, *89*, 083903. [CrossRef]
261. Zinin, P.V.; Bykov, A.A.; Machikhin, A.S.; Troyan, I.A.; Bulatov, K.M.; Mantrova, Y.V.; Batshev, V.I.; Gaponov, M.I.; Kutuza, I.B.; Rashchenko, S.V.; et al. Measurement of the temperature distribution on the surface of the laser heated specimen in a diamond anvil cell system by the tandem imaging acousto-optical filter. *High Press. Res.* **2019**, *39*, 131–149. [CrossRef]
262. Giampaoli, R.; Kantor, I.; Mezouar, M.; Boccato, S.; Rosa, A.D.; Torchio, R.; Garbarino, G.; Mathon, O.; Pascarelli, S. Measurement of temperature in the laser heated diamond anvil cell: Comparison between reflective and refractive optics. *High Press. Res.* **2018**, *38*, 250–269. [CrossRef]
263. Du, Z.; Amulele, G.; Benedetti, L.R.; Lee, K.K. Mapping temperatures and temperature gradients during flash heating in a diamond-anvil cell. *Rev. Sci. Instrum.* **2013**, *84*, 075111. [CrossRef]
264. Manghnani, M.H.; Yagi, T. *Properties of Earth and Planetary Materials at High Pressure and Temperature*; American Geophysical Union: Washington, DC, USA, 1998.
265. Watkins, E.B.; Huber, R.C.; Childs, C.M.; Salamat, A.; Pigott, J.S.; Chow, P.; Xiao, Y.; Coe, J.D. Diamond and methane formation from the chemical decomposition of polyethylene at high pressures and temperatures. *Sci. Rep.* **2022**, *12*, 631. [CrossRef]
266. Gomez-Perez, N.; Rodriguez, J.F.; McWilliams, R.S. Finite element modeling of melting and fluid flow in the laser-heated diamond-anvil cell. *J. Appl. Phys.* **2017**, *121*, 145904. [CrossRef]
267. Dorfman, S.M.; Nabiei, F.; Boukaré, C.-E.; Prakapenka, V.B.; Cantoni, M.; Badro, J.; Gillet, P. Composition and Pressure Effects on Partitioning of Ferrous Iron in Iron-Rich Lower Mantle Heterogeneities. *Minerals* **2021**, *11*, 512. [CrossRef]
268. Geballe, Z.M.; Jeanloz, R. Origin of temperature plateaus in laser-heated diamond anvil cell experiments. *J. Appl. Phys.* **2012**, *111*, 123518. [CrossRef]
269. Cengel, Y.; Boles, M.A.; Boles, M.A. *Thermodynamics: An Engineering Approach: An Engineering Approach*; McGraw-Hill: New York, NY, USA, 2018.
270. Miyajima, N.; Fujino, K.; Funamori, N.; Kondo, T.; Yagi, T. Garnet-perovskite transformation under conditions of the Earth's lower mantle: An analytical transmission electron microscopy study. *Phys. Earth Planet. Inter.* **1999**, *116*, 117–131. [CrossRef]
271. Juarez-Arellano, E.A.; Avdeev, M.; Yakovlev, S.; Lopez-de-la-Torre, L.; Bayarjargal, L.; Winkler, B.; Friedrich, A.; Kharton, V.V. High-pressure behavior and equations of state of the cobaltates $YBaCo_4O_7$, $YBaCo_4O_{7+\delta}$, $YBaCoZn_3O_7$ and $BaCoO_{3-x}$. *J. Solid State Chem.* **2012**, *196*, 209–216. [CrossRef]
272. Haynes, W.M. *CRC Handbook of Chemistry and Physics*; CRC Press LLC: Boca Raton, FL, USA, 2011.
273. Goldsmith, A.; Waterman, T.E.; Hirschhorn, H.J. *Handbook of Thermophysical Properties of Solid Materials*; Macmillan: New York, NY, USA, 1961.

274. Tateno, S.; Hirose, K.; Komabayashi, T.; Ozawa, H.; Ohishi, Y. The structure of Fe-Ni alloy in Earth's inner core. *Geophys. Res. Lett.* **2012**, *39*. [CrossRef]
275. Sist, M.; Fischer, K.F.F.; Kasai, H.; Iversen, B.B. Low-Temperature Anharmonicity in Cesium Chloride (CsCl). *Angew. Chem. Int. Ed.* **2017**, *56*, 3625–3629. [CrossRef]
276. Drebushchak, V.A.; Kovalevskaya, Y.A.; Paukov, I.E.; Surkov, N.V. Low-temperature heat capacity of monoclinic enstatite. *J. Therm. Anal. Calorim.* **2008**, *94*, 493–497. [CrossRef]
277. Funamori, N.; Jeanloz, R.; Miyajima, N.; Fujino, K. Mineral assemblages of basalt in the lower mantle. *J. Geophys. Res. Solid Earth* **2000**, *105*, 26037–26043. [CrossRef]
278. Zeng, Z.; Yang, L.; Zeng, Q.; Lou, H.; Sheng, H.; Wen, J.; Miller, D.J.; Meng, Y.; Yang, W.; Mao, W.L.; et al. Synthesis of quenchable amorphous diamond. *Nat. Commun.* **2017**, *8*, 322. [CrossRef] [PubMed]
279. Zinin, P.V.; Ming, L.C.; Ishii, H.A.; Jia, R.; Acosta, T.; Hellebrand, E. Phase transition in BCx system under high-pressure and high-temperature: Synthesis of cubic dense BC3 nanostructured phase. *J. Appl. Phys.* **2012**, *111*, 114905. [CrossRef]
280. Briggs, R.; Daisenberger, D.; Salamat, A.; Garbarino, G.; Mezouar, M.; Wilson, M.; McMillan, P.F. Melting of Sn to 1 Mbar. *J. Phys. Conf. Ser.* **2012**, *377*, 012035. [CrossRef]
281. Irifune, T.; Susaki, J.-I.; Yagi, T.; Sawamoto, H. Phase transformations in diopside $CaMgSi_2O_6$ at pressures Up to 25 GPa. *Geophys. Res. Lett.* **1989**, *16*, 187–190. [CrossRef]
282. Touloukian, Y.S.; Buyco, E.H. *Thermophysical Properties of Matter: The TPRC Data Series*; S.R.S. Sastry: New York, NY, USA; Washington, DC, USA, 1971; Volume 4, pp. 559–560.
283. Hearne, G.; Bibik, A.; Zhao, J. CO2 laser-heated diamond-anvil cell methodology revisited. *J. Phys. Condens. Matter* **2002**, *14*, 11531–11535. [CrossRef]
284. Heinz, D.L.; Jeanloz, R. Temperature Measurements in the Laser-Heated Diamond Cell. In *High-Pressure Research in Mineral Physics: A Volume in Honor of Syun-iti Akimoto*; Terra Scientific Publishing Company: Tokyo, Japan, 1987; pp. 113–127.
285. Weckert, E. The potential of future light sources to explore the structure and function of matter. *IUCrJ* **2015**, *2*, 230–245. [CrossRef]
286. Kimura, T.; Ohfuji, H.; Nishi, M.; Irifune, T. Melting temperatures of MgO under high pressure by micro-texture analysis. *Nat. Commun.* **2017**, *8*, 15735. [CrossRef]
287. Britvin, S.N.; Vereshchagin, O.S.; Shilovskikh, V.V.; Krzhizhanovskaya, M.G.; Gorelova, L.A.; Vlasenko, N.S.; Pakhomova, A.S.; Zaitsev, A.N.; Zolotarev, A.A.; Bykov, M.; et al. Discovery of terrestrial allabogdanite (Fe,Ni)2P, and the effect of Ni and Mo substitution on the barringerite-allabogdanite high-pressure transition. *Am. Miner.* **2021**, *106*, 944–952. [CrossRef]
288. Forman, R.A.; Piermarini, G.J.; Barnett, J.D.; Block, S. Pressure measurement made by the utilization of ruby sharp-line luminescence. *Science* **1972**, *176*, 284–285. [CrossRef]
289. Syassen, K. Ruby under pressure. *High Press. Res.* **2008**, *28*, 75–126. [CrossRef]
290. Shen, G.; Wang, Y.; Dewaele, A.; Wu, C.; Fratanduono, D.E.; Eggert, J.; Klotz, S.; Dziubek, K.F.; Loubeyre, P.; Fat'yanov, O.V.; et al. Toward an international practical pressure scale: A proposal for an IPPS ruby gauge (IPPS-Ruby2020). *High Press. Res.* **2020**, *40*, 299–314. [CrossRef]
291. Tuschel, D. Photoluminescence spectroscopy using a Raman spectrometer. *Spectroscopy* **2016**, *31*, 14–21.
292. Vos, W.L.; Schouten, J.A. On the temperature correction to the ruby pressure scale. *J. Appl. Phys.* **1991**, *69*, 6744–6746. [CrossRef]
293. Yen, J.; Nicol, M. Temperature dependence of the ruby luminescence method for measuring high pressures. *J. Appl. Phys.* **1992**, *72*, 5535–5538. [CrossRef]
294. Chijioke, A.D.; Nellis, W.J.; Soldatov, A.; Silvera, I.F. The ruby pressure standard to 150 GPa. *J. Appl. Phys.* **2005**, *98*, 114905. [CrossRef]
295. Araújo, A. Multi-spectral pyrometry—A review. *Meas. Sci. Technol.* **2017**, *28*, 082002. [CrossRef]
296. Hasegawa, A.; Yagi, T.; Ohta, K. Combination of pulsed light heating thermoreflectance and laser-heated diamond anvil cell for in-situ high pressure-temperature thermal diffusivity measurements. *Rev. Sci. Instrum.* **2019**, *90*, 074901. [CrossRef]
297. Benedetti, L.R.; Guignot, N.; Farber, D.L. Achieving accuracy in spectroradiometric measurements of temperature in the laser-heated diamond anvil cell: Diamond is an optical component. *J. Appl. Phys.* **2007**, *101*, 013109. [CrossRef]
298. Weir, C.E.; Lippincott, E.R.; Van Valkenburg, A.; Bunting, E.N. Infrared Studies in the 1- to 15-Micron Region to 30,000 Atmospheres. *J. Res. Nat. Bur. Stand. A Phys. Chem.* **1959**, *63*, 55–62. [CrossRef]
299. Spetzler, H.; Shen, A.; Chen, G.; Herrmannsdoerfer, G.; Schulze, H.; Weigel, R. Ultrasonic measurements in a diamond anvil cell. *Phys. Earth Planet. Inter.* **1996**, *98*, 93–99. [CrossRef]
300. Shiell, T.B.; McCulloch, D.G.; Bradby, J.E.; Haberl, B.; Boehler, R.; McKenzie, D.R. Nanocrystalline hexagonal diamond formed from glassy carbon. *Sci. Rep.* **2016**, *6*, 37232. [CrossRef]
301. Peng, F.; Sun, Y.; Pickard, C.J.; Needs, R.J.; Wu, Q.; Ma, Y. Hydrogen Clathrate Structures in Rare Earth Hydrides at High Pressures: Possible Route to Room-Temperature Superconductivity. *Phys. Rev. Lett.* **2017**, *119*, 107001. [CrossRef]
302. Drozdov, A.P.; Kong, P.P.; Minkov, V.S.; Besedin, S.P.; Kuzovnikov, M.A.; Mozaffari, S.; Balicas, L.; Balakirev, F.F.; Graf, D.E.; Prakapenka, V.B.; et al. Superconductivity at 250 K in lanthanum hydride under high pressures. *Nature* **2019**, *569*, 528–531. [CrossRef]
303. Wang, H.; Tse, J.S.; Tanaka, K.; Iitaka, T.; Ma, Y. Superconductive sodalite-like clathrate calcium hydride at high pressures. *Proc. Natl. Acad. Sci. USA* **2012**, *109*, 6463–6466. [CrossRef]

304. Kong, P.; Minkov, V.S.; Kuzovnikov, M.A.; Drozdov, A.P.; Besedin, S.P.; Mozaffari, S.; Balicas, L.; Balakirev, F.F.; Prakapenka, V.B.; Chariton, S.; et al. Superconductivity up to 243 K in the yttrium-hydrogen system under high pressure. *Nat. Commun.* **2021**, *12*, 5075. [CrossRef]
305. Drozdov, A.P.; Eremets, M.I.; Troyan, I.A.; Ksenofontov, V.; Shylin, S.I. Conventional superconductivity at 203 kelvin at high pressures in the sulfur hydride system. *Nature* **2015**, *525*, 73–76. [CrossRef]
306. Matsumoto, R.; Yamamoto, S.; Adachi, S.; Sakai, T.; Irifune, T.; Takano, Y. Diamond anvil cell with boron-doped diamond heater for high-pressure synthesis and in situ transport measurements. *Appl. Phys. Lett.* **2021**, *119*, 053502. [CrossRef]
307. Ke, F.; Wang, C.; Jia, C.; Wolf, N.R.; Yan, J.; Niu, S.; Devereaux, T.P.; Karunadasa, H.I.; Mao, W.L.; Lin, Y. Preserving a robust CsPbI3 perovskite phase via pressure-directed octahedral tilt. *Nat. Commun.* **2021**, *12*, 461. [CrossRef]